THE MINISTRY OF SCIENCE AND HIGHER EDUCATION OF THE RUSSIAN FEDERATION

ISSN 2687-0517

Computing, Telecommunications and Control

Vol. 16, No. 4
2023

Peter the Great St. Petersburg
Polytechnic University
2023

The journal is included in the List of Leading PeerReviewed Scientific Journals and other editions to publish major findings of PhD theses for the research degrees of Doctor of Sciences and Candidate of Sciences.

Open access journal is to publish articles of a high scientific level covering advanced experience, research results, theoretical and practical problems of informatics, electronics, telecommunications, and control.

The journal is indexed by Ulrich's Periodicals Directory, Google Scholar, EBSCO, ProQuest, Index Copernicus, VINITI RAS Abstract Journal (Referativnyi Zhurnal), VINITI RAS Scientific and Technical Literature Collection, Russian Science Citation Index (RSCI) database Scientific Electronic Library and Math-Net.ru databases.

The journal is registered with the Federal Service for Supervision in the Sphere of Telecom, Information Technologies and Mass Communications (ROSKOMNADZOR). Certificate ЭЛ No. ФС77-77378 issued 25.12.2019.

Editorial office

Dr. Sc., Professor A.S. Korotkov – Editor-in-Chief;

E.A. Kalinina – literary editor, proofreader; G.A. Pyshkina – editorial manager; A.A. Kononova – computer layout; D.Yu. Alekseeva – English translation.

Address: 195251 Polytekhnicheskaya Str. 29, St. Petersburg, Russia.

+7 (812) 552-6216, e-mail: infocom@spbstu.ru

Release date: 29.12.2023

МИНИСТЕРСТВО НАУКИ И ВЫСШЕГО ОБРАЗОВАНИЯ РОССИЙСКОЙ ФЕДЕРАЦИИ

ISSN 2687-0517

Информатика, телекоммуникации и управление

Том 16, № 4
2023

Санкт-Петербургский политехнический
университет Петра Великого
2023

ИНФОРМАТИКА, ТЕЛЕКОММУНИКАЦИИ И УПРАВЛЕНИЕ

Журнал с 2002 года входит в Перечень ведущих рецензируемых научных журналов и изданий, в которых должны быть опубликованы основные результаты диссертаций на соискание ученой степени доктора и кандидата наук.

Сетевое издание открытого доступа публикует статьи высокого научного уровня, освещающие передовой опыт, результаты НИР, теоретические и практические проблемы информатики, электроники, телекоммуникаций, управления.

Сведения о публикациях представлены в Реферативном журнале ВИНИТИ РАН, в международной справочной системе «Ulrich`s Periodical Directory», в Российской государственной библиотеке. В базах данных: Российский индекс научного цитирования (РИНЦ), Google Scholar, EBSCO, Math-Net.Ru, ProQuest, Index Copernicus.

Журнал зарегистрирован Федеральной службой по надзору в сфере информационных технологий и массовых коммуникаций (Роскомнадзор). Свидетельство о регистрации ЭЛ № ФС77-77378 от 25.12.2019.

Учредитель и издатель: Санкт-Петербургский политехнический университет Петра Великого, Санкт-Петербург, Российская Федерация.

Редакция журнала

д-р техн. наук, профессор А.С. Коротков – главный редактор;

Е.А. Калинина – литературный редактор, корректор; Г.А. Пышкина – ответственный секретарь, выпускающий редактор;

А.А. Кононова – компьютерная вёрстка; Д.Ю. Алексеева – перевод на английский язык.

Адрес редакции: Россия, 195251, Санкт-Петербург, ул. Политехническая, д. 29.

Тел. редакции +7(812) 552-62-16, e-mail: infocom@spbstu.ru

Дата выхода: 29.12.2023

Contents

Содержание

Computing, Telecommunication and Control, 2023, Vol. 16, No. 4, Pp. 7–17.
Информатика, телекоммуникации и управление. 2023. Том 16, № 4. С. 7–17.

Circuits and Systems for Receiving, Transmitting and Signal Processing

Устройства и системы передачи, приема и обработки сигналов

Research article
DOI: https://doi.org/10.18721/JCSTCS.16401
UDC 681.775

A METHOD FOR EVALUATING THE LIGHTING PARAMETERS OF DIGITAL VIDEO PROJECTORS IN REAL OPERATING CONDITIONS

S.V. Perelygin[1,2] ✉ , *K.K. Gudinov*[1], *S.V. Kuklin*[1], *A.P. Parfenov*[3]

[1] St. Petersburg State University of Film and Television, St. Petersburg, Russian Federation;

[2] The Bonch-Bruevich Saint Petersburg State University of Telecommunications, St. Petersburg, Russian Federation;

[3] International Film Festival "Message to Man", St. Petersburg, Russian Federation

✉ sergey.perelygin@gmail.com

Abstract. The article briefly examines modern standards regulating the measurement of lighting parameters of digital video projectors. It is pointed out that existing standards do not have the ability to take into account the settings of video projectors that are performed after factory calibration at the places of their operation. The authors proposed a method for setting and measuring the output lighting parameters of a video projector, which affect the quality of the resulting image, in a real room other than a completely dark room. Following this method, it is possible to obtain reliable values of the lighting parameters of the video projector directly in the room where it is operated, which is especially important for the multimedia video projector market. This takes into account the operating conditions and service life of the video projector, and in particular factors such as the imposition of external highlights on the illumination of the screen and the design features of the lighting and projection systems of projectors. An experiment is described to measure the luminous flux, contrast and brightness of eight video projectors for different market segments with different service life. It is concluded that the obtained values of lighting parameters are more reliable in comparison with those indicated by projector manufacturers in the specifications.

Keywords: digital video projector, luminous flux, contrast, illumination, calibration

Citation: Perelygin S.V., Gudinov K.K., Kuklin S.V., Parfenov A.P. A method for evaluating the lighting parameters of digital video projectors in real operating conditions. Computing, Telecommunications and Control, 2023, Vol. 16, No. 4, Pp. 7–17. DOI: 10.18721/JCSTCS.16401

Научная статья
DOI: https://doi.org/10.18721/JCSTCS.16401
УДК 681.775

МЕТОД ОЦЕНКИ СВЕТОТЕХНИЧЕСКИХ ПАРАМЕТРОВ ЦИФРОВЫХ ВИДЕОПРОЕКТОРОВ В РЕАЛЬНЫХ УСЛОВИЯХ ЭКСПЛУАТАЦИИ

С.В. Перелыгин[1,2] ✉ , *К.К. Гудинов*[1], *С.В. Куклин*[1], *А.П. Парфёнов*[3]

[1] Санкт-Петербургский государственный институт кино и телевидения, Санкт-Петербург, Российская Федерация;

[2] Санкт-Петербургский государственный университет телекоммуникаций им. проф. М.А. Бонч-Бруевича, Санкт-Петербург, Российская Федерация;

[3] Международный кинофестиваль «Послание к человеку», Санкт-Петербург, Российская Федерация

✉ sergey.perelygin@gmail.com

Аннотация. В статье кратко рассмотрены современные стандарты, регламентирующие измерение светотехнических параметров цифровых видеопроекторов. Указано на отсутствие возможности у существующих стандартов учитывать настройки видеопроекторов, выполняемые уже после заводской калибровки в местах их эксплуатации. Авторами предложен метод настройки и измерения выходных светотехнических параметров видеопроектора, которые влияют на качество получаемого изображения, в условиях реального помещения, отличного от абсолютно тёмной комнаты. Следуя данному методу, можно получить достоверные значения светотехнических параметров видеопроектора непосредственно в помещении, где он эксплуатируется, что особенно актуально для рынка мультимедийных видеопроекторов. При этом учитываются условия эксплуатации и срок службы видеопроектора, и в частности такие факторы, как наложение внешних засветок на освещённость экрана и конструкционные особенности работы осветительно-проекционных систем проекторов. Описан эксперимент по измерению светового потока, контрастности и яркости восьми видеопроекторов для различных сегментов рынка с разным сроком эксплуатации. Сделан вывод о большей достоверности полученных значений светотехнических параметров в сравнении с указываемыми производителями проекторов в спецификациях.

Ключевые слова: цифровой видеопроектор, световой поток, контрастность, освещённость, калибровка

Для цитирования: Perelygin S.V., Gudinov K.K., Kuklin S.V., Parfenov A.P. A method for evaluating the lighting parameters of digital video projectors in real operating conditions // Computing, Telecommunications and Control. 2023. Т. 16, № 4. С. 7–17. DOI: 10.18721/JCSTCS.16401

Introduction

Digital video projection technologies today are widely used in schools, offices, home and commercial cinemas, in university classrooms and in many areas where visual information is required to be displayed on the big screen [1–9].

Appropriate standards have been developed to describe the technical characteristics of digital video projectors.

In accordance with the DCSS (Digital Cinema System Specification v1) approved by the DCI (Digital Cinema Initiatives) association of leading Hollywood film studios in 2005 [10], recommendations of the Society of Film and Television Engineers SMPTE431-1-2006 [11] and SMPTE RP 431-2: 2011 [12], International Organization for Standardization (ISO) and International Electrotechnical Commission

Fig. 1. Test image for calibration of projector before measurements according to GOST IEC 61947-1-2014 [13]

(IEC) developed standards to describe the technical characteristics of video projectors, as well as their specifications. Measured parameters are given in the ANSI (*A*merican *N*ational *S*tandards *I*nstitute) system, for example, ANSI lumen, ANSI contrast.

In the CIS countries, the Euro-Asian Council for standardization, metrology and certification (EASC) deals with standardization and regulatory documentation of technical devices. In 2016, the EASC standards GOST IEC 61947-1-2014 and GOST IEC 61947-2-2014 were put into effect as a national standard of the Russian Federation. They establish requirements for measurement and documentation of key operating parameters for electronic projection systems (projectors) with constant and variable resolution, respectively [13, 14]. Next, we will focus on the interstate standard GOST IEC 61947-1-2014 (identical to the international standard IEC 61947-1: 2002).

The bibliographic search carried out by the authors revealed *the absence* of scientific publications that would contain recommendations on setting up and measuring the lighting parameters of the projector in *a real room*. A separate standard regulating the corresponding setup and measurement procedures in *real premises* has *not been developed* at the moment either. Therefore, the experience gained in the course of many years of practice in the field of video projection equipment maintenance at entertainment events and the recommendations of specialists (enthusiasts) in this field are *relevant*. However, despite the widespread dissemination of such recommendations, both among lighting engineers (an example is *A.P. Parfenov*, one of the authors of this article) and on the Internet, sources containing them cannot be attributed to scientific works. The authors of the article proposed the simplest and most effective method for setting up and measuring the lighting parameters of video projectors in real operating conditions. This method allows to assess the actual condition of video projectors, regardless of their service life.

Setting up and measuring lighting parameters of a video projector in laboratory conditions

According to [13], before starting measurements, the projector brightness and contrast controls shall be calibrated using the test image shown in Fig. 1 as follows: the brightness shall be set to the maximum value at which the maximum number of brightness bands corresponding to brightness levels of 0%, 5%, 10%, 15% (upper row) is discernible. The contrast should increase from the minimum value to the maximum, at which the maximum number of brightness bands corresponding to brightness levels of 85%, 90%, 95%, 100% (lower row) is visible and distinguishable, or until the image brightness stops rising due to the automatic brightness adjustment scheme of the projector.

After calibration of the video projector, the main parameters determining the quality of the obtained image are measured [13].

To measure light, a completely white image is projected onto the screen. Screen illumination is measured using a light meter for nine areas in the center of each equal rectangle (1÷9 points in Fig. 2). Next, the illumination values are averaged and multiplied by the screen area value. The light flux value obtained in this way is given in ANSI-lumens.

Contrast is determined using two methods. The first of them is to measure the ratio of screen brightness when projecting a white and black field (Sequential Full On / Full Off, Full) in a completely darkened room. The Full On/Off contrast indicator is not informative, since the brightness of the black field

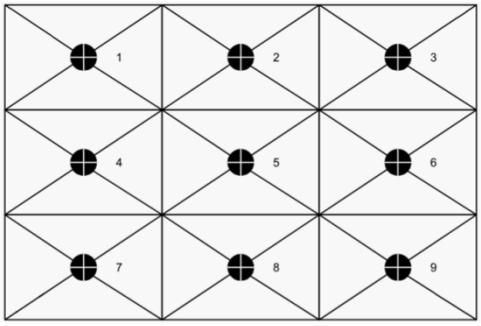

Fig. 2. Grid with points for measuring image illumination in accordance with GOST IEC 61947-1-2014 [13]

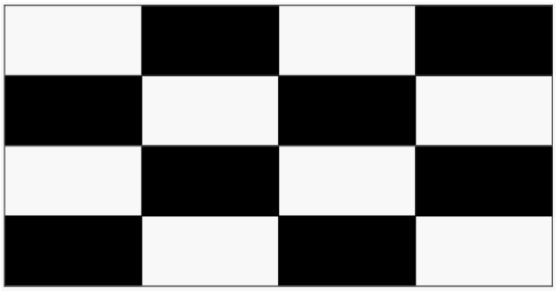

Fig. 3. Test image for measuring contrast and black level in accordance with GOST IEC 61947-1-2014 [13]

can be significantly reduced, for example by automatically diaphragm (decrease in aperture) of the lens. Adaptive aperture control is always used by manufacturers declaring thousands of contrast of their projectors [2], for example, 3000:1 or more.

For a more reliable measurement of the contrast of the projector the second method is used. It involves – measuring a ratio of the total (or average) brightness of white and black rectangles on the screen when projecting a checkerboard (Intra-frame Checkerboard) (Fig. 3). The contrast value obtained in this way is called ANSI contrast.

Since some multimedia projectors use color filters with a transparent sector to display colors [2], often the maximum brightness of a white image is more than the sum of the maximum brightness of images of primary colors. Therefore, in addition to prescribed measurements [13] of WLO values (*W*hite *L*ight *O*utput – output luminous flux), to estimate the total useful light flux of the projector it is necessary to measure the color light flux CLO (*C*olor *L*ight *O*utput). To measure it, test images are supplied to the screen, consisting of nine rectangles of RGB primary colors in three different combinations (Fig. 4) [15]. A total of 27 light measurements are carried out. For each measured color, the average illumination value is taken, then the obtained illuminations are added.

If WLO value exceeds CLO value, then the projector uses the so-called "white gain" (white boost), which leads to inaccuracies in color transmission compared to standards widely used for digital images such as sRGB and BT.709/BT.1886 [15].

The method of measuring the lighting parameters of a tuned video projector in a real room

WLO and CLO values specified by the projector manufacturers in the specification, cannot be a factor determining the quality of the projected image, since the real projected image often achieves the best quality with *additional settings* (for example, color correction and color balance), which can significantly reduce the output luminous flux. Therefore, during the experiment, the authors of the article will also measure the output WLO and CLO luminous flux of projectors after making settings in accordance with [13].

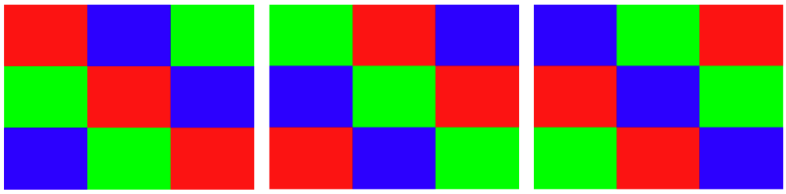

Fig. 4. Test Images for CLO Measurement

Fig. 5. Test image for additional black level adjustment of the projector

As already noted, *no separate recommendations* have been developed for measuring the lighting parameters of the projector in a real room. The authors of the article propose a method for *setting up* and *measuring* the parameters of video projectors in real operating conditions based on the method presented in [16]. We emphasize that the original source focuses only on *adjusting* the color rendition of the video projector *without* any additional objective or subjective *assessments*, as well as *without* specifying the *conditions* for using this method and *the service life* of the video projector at the time of adjustment.

It will be appropriate to compare the test images discussed in [16] with the test calibration images specified in the standard [13], and then use them to configure the video projector and then to perform measurements of its lighting parameters.

For the correct display of dark tones, we adjust the projector according to the image shown in Fig. 5. The image consists of squares of different gray levels (white intensity varies from "0" to "255") on a black background. The brightness and contrast settings of the projector are set to the maximum position at which a square with a gray level of "5" is visible and distinguishable, which corresponds to about 2% brightness level, unlike calibration images [13], following in brightness increments of 5%.

To correctly display light tones, we adjust the projector according to the image shown in Fig. 6. The image consists of white-gray "chess" patterns of various levels of gray (white intensity in the gray parts of the pattern varies from "200" to "254") on a white background. The brightness and contrast settings of the projector are set to the maximum position at which a pattern with a white intensity of "251" is visible and distinguishable, which corresponds to about 98% brightness level, again unlike calibration images [13], following in brightness increments of 5%.

The final part of the setup is carried out using the image shown in Fig. 7. The image consists of bands of main (R, G, B) and additional (C, Y, M) colors of various brightness levels. The brightness and contrast settings of the projector are adjusted so that the brightness levels "1" and "2," as well as "30" and "32" of the maximum number of colors are visible in the image.

According to SMPTE, in rooms with a large amount of sunlight (for example, in school and lecture classes), the brightness in the center of the screen should be more than 170 cd/m^2 (50 ft-lb). You can reduce the required image brightness using light-tight curtains. In such a darkened room, brightness from 100 cd/m^2 (30 ft-Lb) will be enough [11, 17].

Fig. 6. Test image for additional white level adjustment of the projector

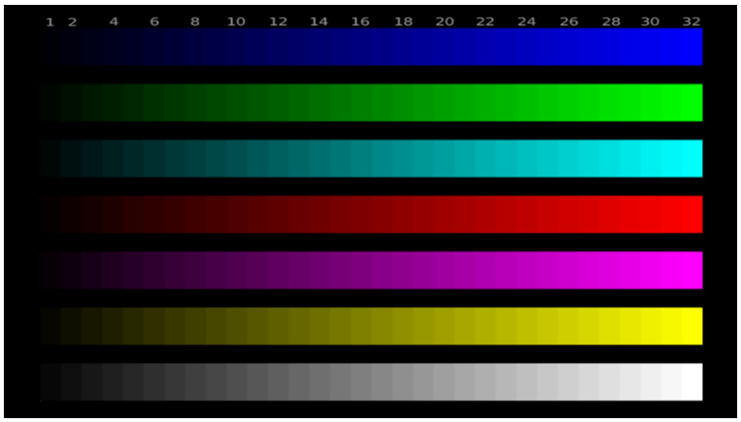

Fig. 7. Test image to further adjust the projector by levels of primary and secondary colors

The experiment on measuring the parameters of the output light flux by the authors of the article will be carried out not in ideal conditions of an absolutely dark room, but in real rooms, therefore, the readings of the light meter at each measurement have three components [18]: $\mathbf{E}_{\mathbf{DR}}$ – direct component of illumination, created directly by the projector light flux, $\mathbf{E}_{\mathbf{RF}}$ – reflected component of illumination, created as a result of multiple reflections from the surfaces of the room and screen, and $\mathbf{E}_{\mathbf{BG}}$ – background component of illumination, which takes place due to the impossibility of completely eliminating the ingress of light through the doors and windows of the room:

$$\mathbf{E}_{\Sigma} = \mathbf{E}_{\mathbf{DR}} + \mathbf{E}_{\mathbf{RF}} + \mathbf{E}_{\mathbf{BG}}, \quad (1)$$

where $\mathbf{E}_{\Sigma}$ is the total (full) measured illumination indicated by a light meter located in the plane of the screen. The combination of reflected $\mathbf{E}_{\mathbf{RF}}$ and background $\mathbf{E}_{\mathbf{BG}}$ components of illumination is designated as $\mathbf{E}_{\mathbf{SD}}$ (side illumination).

The screen may be located close to the different reflecting surfaces of the room by each edge thereof. Therefore, the combination of reflected and background light components cannot be considered evenly distributed across the screen and side illumination should be evaluated for each test rectangle separately. For this, the direct light flux from the projector is blocked by a light-impermeable object in such a way that the light meter in the plane of the screen is in the shadow of this object. Since illumination is an additive value, the direct contribution of the video projector to the illumination level of the corresponding area of the screen will be equal to the difference between two consecutive measurements:

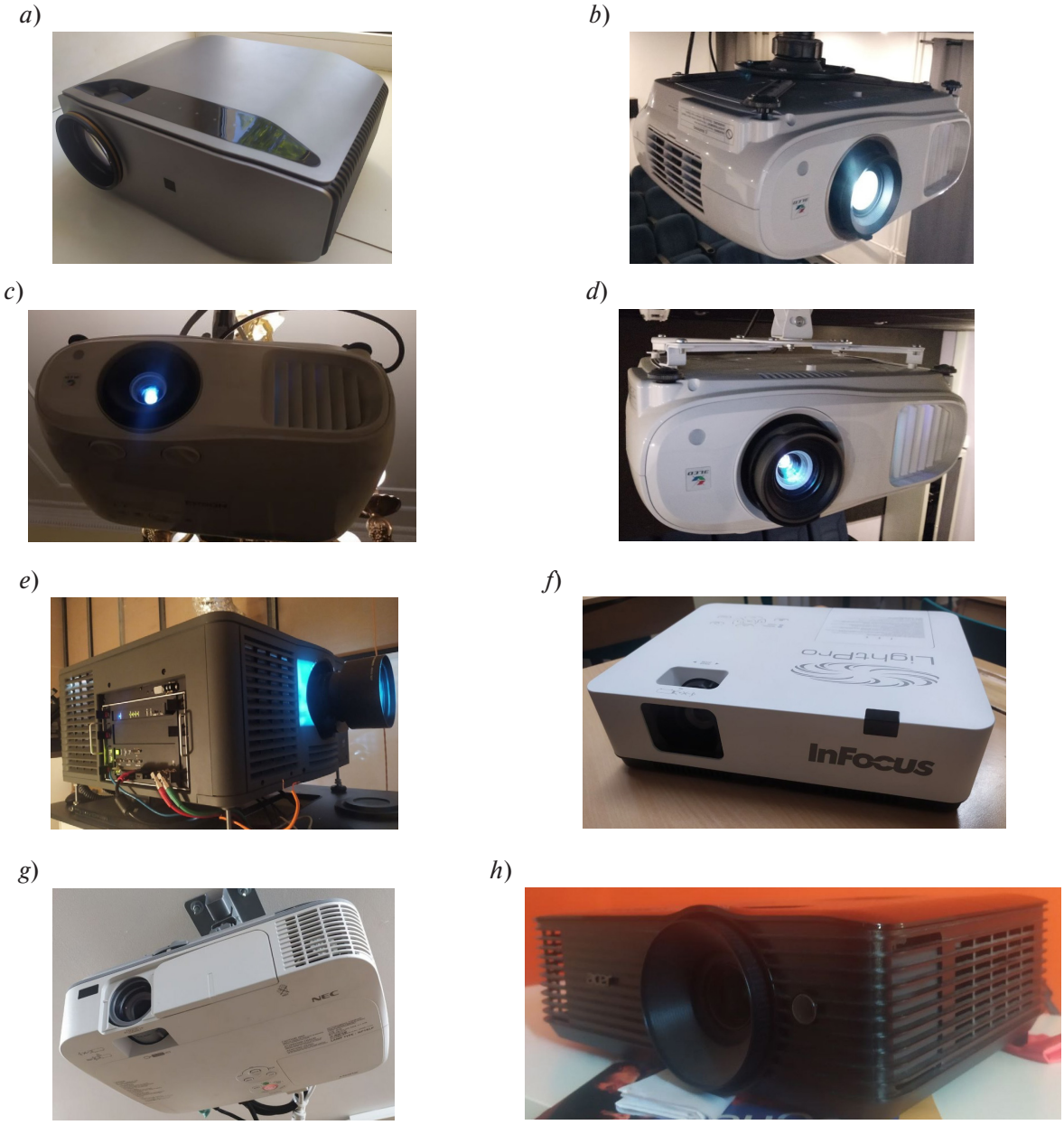

Fig. 8. Tested video projectors and their service life: *a* – UNIC YG-620 (home cinema, new), *b* – EPSON EH-TW6800 (cinema center «Dom Kino», «White» hall, 4 years), *c* – EPSON EH-TW6800 (cinema center «Dom Kino», «Small» hall, 4 years), *d* – EPSON EH-TW7000 (cinema center «Dom Kino», «Lilac» hall, 2 years), *e* – Christie CP2210 (cinema center «Dom Kino», «Blue» hall, 13 years), *f* – InFocus In1026 (Gymnasium of St. Ambrose of Optina, assembly hall, new), *g* – NEC M300W (Gymnasium of St. Ambrose of Optina, classroom, less than a year), *h* – Acer X118AH (coworking «GrowUp», meeting room №1, less than a year)

$$\mathbf{E}_{\mathbf{DR}} = \mathbf{E}_{\Sigma} - \mathbf{E}_{\mathbf{SD}}. \quad (2)$$

Experiment on measuring the lighting parameters of a video projector in a real room

In the experimental part, the parameters of the output light flux of eight projectors were measured in real conditions of their operation. Photos of the tested projectors indicating the service life from the beginning of operation are shown in Fig. 8, *a*–*h*.

Table 1 shows the main technical characteristics of the tested projectors declared by the manufacturers.

To measure the output light parameters of the projectors, measuring devices produced by the "TKA" scientific and technical enterprise [19] were used: a combined "TKA-PKM 02" device for measuring screen illumination and "TKA-YAR" brightness meters for measuring brightness.

Test images (Fig. 1, 3–7) were recorded on a USB flash drive connected directly to video projectors and played back by projectors using the built-in control menu. For each projector, the following values were measured: output luminous flux (WLO), color luminous flux (CLO), ANSI contrast, brightness of the resulting image for the center of the screen (Table 2). WLO, CLO and brightness were measured for each projector twice: with calibration according to GOST IEC 61947-1-2014 (designation "GOST" in Table 2) and after additional configuration, the method of which was described earlier (designation "Additional" in Table 2). All measurements were made at the maximum power consumption mode of the lamp.

Table 1

Main technical characteristics of the tested projectors

Video projector	Imaging technology	Number of light modulating matrices	Light source	Maximum power of the light source, W	Service life of the light source in normal mode, h	Service life of light source in economy mode, h	Projector resolution	Output luminous flux (WLO), lm	Contrast
UNIC YG-620	LCD	1	LED	140	20000	50000	1920×1080 (Full HD)	6500	3000:1
Epson EH-TW6800	LCD	3	high-pressure mercury lamp	250	3500	5000	1920×1080 (Full HD)	2700	120000:1
Epson EH-TW7000	LCD	3		250	3500	5000	4096×2160 (4K PRO-UHD)	3000	40000:1
Christie CP2210	DLP	3	ultra-high pressure xenon lamp	1600	3000	–	2048×1080 (2K)	12000	2000:1
InFocus In1026	LCD	3	high-pressure mercury lamp	240	10000	20000	1280×800	4200	50000:1
NEC M300W	LCD	3		230	4000	5000	1280×800	3000	2000:1
Acer X118AH	DLP	1		203	4000	10000	800×600	3600	20000:1

Results of the experiment and their analysis

When comparing the measurement results (Table 2) and the technical characteristics of the video projectors (Table 1), it can be seen that ***none*** of the tested projectors produces the WLO luminous flux declared by the manufacturer in the specification during calibration according to GOST [13]. There are several reasons for this. *Firstly*, some test projectors have a long operating history, which affects the reduction in the efficiency of light sources and light modulating matrices. *Secondly*, manufacturers

Table 2

Results of measurements of characteristics of test projectors

Projector	WLO, ANSI-lm		CLO, ANSI-lm		Brightness, cd/m²		ANSI-contrast, k:1
	GOST	Add.	GOST	Add.	GOST	Add.	
UNIC YG-620	280	270	250	240	120	110	300:1
EPSON EH-TW6800 (N1)	320	260	310	250	35	30	100:1
EPSON EH-TW6800 (N2)	420	340	380	310	50	42	35:1
EPSON EH-TW7000	1180	970	1170	930	61	50	26:1
Christie CP2210	1890	1490	1870	1490	60	55	100:1
InFocus In1026	2910	2840	2870	2720	320	300	90:1
NEC M300W	1050	840	1050	800	120	110	90:1
Acer X118AH	1070	930	390	380	110	100	11:1

indicate the maximum amount of light flux, which must be reduced to obtain a high-quality image on the screen.

After additional configuration most of the tested projectors display an image of sufficient brightness for their purposes on the screen except the EPSON EH-TW6800 projector which gives the brightness of the image significantly lower than the SMPTE minimum for digital cinema of 37.8 cd/m².

The CLO value is approximately equal to the WLO value for all tested projectors except the Acer X118AH single-matrix DLP projector (CLO is approximately 40% of WLO).

The ANSI contrast values measured during the experiment are orders of magnitude less than the contrast indicators declared by the manufacturers in the specifications. Of the four tested projectors used for commercial film screenings, only two correspond to the minimum allowed ANSI contrast level of 100:1 according to SMPTE RP 431-2: 2011.

Conclusion

To date, there are *no practical* recommendations for measuring the parameters of a video projector in real conditions of its operation. Specifications of video projectors are often compiled by manufacturers taking into account the further need for the product to be competitive in the market, therefore, the output lighting values indicated in them, measured in laboratory conditions, fail to correctly characterize the parameters of the actually projected image.

In addition to the methods prescribed by the GOST IEC 61947-1-2014 for measuring the output lighting values of video projectors, the authors have proposed their *own* method for measuring these values. The method can be used in relation to video projectors belonging to various market segments, directly in the premises where the projector is operated (i.e., other than laboratory conditions of an ideally dark room), taking into account its service life.

The results of the experiment show that when calibrated according to GOST IEC 61947-1-2014, the luminous flux drops to 60–70% of the maximum, and with additional calibration – down to 50% (!). WLO values with additional configuration of the projector, desirable for obtaining the best image quality, are on average 13% lower than those measured according to GOST IEC 61947-1-2014.

Thus, the proposed method takes into account factors such as the imposition of external illumination on the screen illumination and the design features of the lighting and projection systems of projectors during their use. The method allows additional adjustment of video projectors with subsequent measurements of their output lighting values. This setting makes it possible to obtain the best image quality directly at the place where the projector is installed and used and, in fact, is a clarification of the requirements of the standard [13] for real operating conditions of the projector. The output lighting values of the video projector measured using this method turn out to be more *reliable* than those indicated by the projector manufacturers in the specifications. This factor is especially relevant for multimedia video projectors that have been in operation for a long time and allow the user realistically assess the condition of the video projector and make a timely decision about its replacement.

REFERENCES

1. **Kuklin S.V.** Technique of digital film and video screening: tutorial. SPb.: SPbGICiT, 2017.

2. **Kuklin S.V.** Optical projection systems: tutorial. St. Petersburg: SPbGUKiT, 2012.

3. **Kuklin S.V.** Light sources for film and video projection: tutorial. St. Petersburg: SPbGUKiT, 2013.

4. LCD, LCoS, or DLP: Choosing a Projector Imaging Technology Available: https://www.projector-central.com/Digital-Projector-Imaging-Technologies-Explained.htm, free. English Language (accessed 01.09.2023)

5. **Douglass M.R.** Lifetime estimates and unique failure mechanisms of the Digital Micromirror Device (DMD) – 1998 IEEE International Reliability Physics Symposium Proceedings. 36th Annual, 1998.

6. **Bachels T., Schmitt K., Shadt M.N., et al.** Advanced Electronic Color Switch for Time-Sequential Projection, SID' 01 Digest, 2001, Vol. 32, Pp. 1080–1083.

7. **Flesch P.** Light and Light Sources: High Intensity Discharge Lamps. Springer-Verlag, 2006.

8. **Shih-Fang Liao.** Perceived Brightness of LED Projector. SID Symposium Digest of Technical Papers, 2009, Vol. 40 (1), Pp. 262.

9. **Yamamoto K.** Laser display technologies and their applications. – Advanced Optical Technologies, 2012, No. 6, Pp. 483–488.

10. The official website of Hollywood's leading film studios, Digital Cinema Initiatives (DCI). Available: http://www.dcimovies.com, free. English Language (accessed 30.08.2023).

11. SMPTE 431-1-2006. SMPTE Standard for D-Cinema Quality – Screen Luminance Level, Chromaticity and Uniformity. The Society of Motion Picture and Television Engineers, 2006.

12. SMPTE RP 431-2:2011. SMPTE Recommended Practice. D-Cinema Quality – Reference Projector and Environment. The Society of Motion Picture and Television Engineers, 2011.

13. GOST IEC 61947-1-2014. Electronic projection: measurement and documentation of the key performance criterion. Part 1: projectors with constant resolution. M.: Standardinform, 2018.

14. GOST IEC 61947-2-2014. Electronic projection: measurement and documentation of the key performance criterion. Part 2: Variable resolution projectors. M.: Standardinform, 2016.

15. **Poynton Charles, LeHoty David A.** Invited Paper: Color/White Light Output, Luminance Contours, and Colour Volume. – SID Symposium Digest of Technical Papers, 2020, No. 1, Vol. 51, Pp. 730.

16. **Ooi Jayce.** How to Setup Projector Contrast, Brightness, Colour for Best Picture? – Projector Calibration Guide [Electronic resource]. Available: https://www.jayceooi.com/calibrate-projector/, free. English Language (accessed: 05.09.2023)

17. **Pickus Scott.** Display Brightness vs. Ambient Light [Electronic resource]. Available: https://www.dynascandisplay.com/blog/display-brightness-vs-ambient-light/, free. English Language (accessed 30.08.2023).

18. Calculation of illumination from sources of various types: laboratory workshop for students of the specialty 1-38 01 02 “Optical-electronic and laser devices and systems” specialization 1-38 01 02 04 “Lighting engineering and light sources” comp.: A.S. Kozeruk, A.V. Grishchenko. Minsk: BNTU, 2020.

19. The official website of the scientific and technical enterprise “TKA” Available: https://www.tkaspb.ru/free. English Language (accessed 22.08.2023).

INFORMATION ABOUT AUTHORS / СВЕДЕНИЯ ОБ АВТОРАХ

Perelygin Sergey V.
Перелыгин Сергей Васильевич
E-mail: sergey.perelygin@gmail.com

Gudinov Konstantin K.
Гудинов Константин Кимович
E-mail: kvakg@mail.ru

Kuklin Sergey V.
Куклин Сергей Владимирович
E-mail: kuklinsv57@mail.ru

Parfenov Alexander P.
Парфёнов Александр Павлович
E-mail: parffenof@yandex.ru

Submitted: 27.10.2023; Approved: 18.12.2023; Accepted: 21.12.2023.
Поступила: 27.10.2023; Одобрена: 18.12.2023; Принята: 21.12.2023.

Computing, Telecommunication and Control, 2023, Vol. 16, No. 4, Pp. 18–27.
Информатика, телекоммуникации и управление. 2023. Том 16, № 4. С. 18–27.

Software of Computer, Telecommunications and Control Systems

Программное обеспечение вычислительных, телекоммуникационных и управляющих систем

Research article
DOI: https://doi.org/10.18721/JCSTCS.16402
UDC 004.67

NEW METHODS FOR EFFICIENT ENERGY MANAGEMENT OF A SOLAR VEHICLE ON A FIXED ROUTE

I.A. Selin ✉

Peter the Great St. Petersburg Polytechnic University,
St. Petersburg, Russian Federation

✉ selin_ia@spbstu.ru

Abstract. This paper is devoted to the problem of efficient energy use on a fixed route for solar car racing. Solar cars are electric vehicles that can charge the battery while traveling using a built-in solar array. Solar car races are characterized by very long distances and prohibition of wall charging: vehicles can only be charged using solar energy. This alone creates a serious energy shortage, but coupled with the main goal of finishing in the shortest possible time, the task becomes even more complex. Thus, proper power management is the key to success. Since optimization of power management strategy is a computationally intensive process, modified route representation and use of automatic differentiation are advised to raise the performance of the optimization process. The proposed methods are implemented in the SPbPUStrat software solution, which is capable of solving the problem in a short time: this allows the strategy to be recalculated in full upon request.

Keywords: solar car, strategy, power management strategy, optimization, route representation

Citation: Selin I.A. New methods for efficient energy management of a solar vehicle on a fixed route. Computing, Telecommunications and Control, 2023, Vol. 16, No. 4, Pp. 18–27. DOI: 10.18721/JCSTCS.16402

Научная статья
DOI: https://doi.org/10.18721/JCSTCS.16402
УДК 004.67

НОВЫЕ МЕТОДЫ ОБЕСПЕЧЕНИЯ ЭФФЕКТИВНОГО ИСПОЛЬЗОВАНИЯ ЭНЕРГИИ СОЛНЦЕМОБИЛЕМ НА ЗАДАННОМ МАРШРУТЕ

И.А. Селин ✉

Санкт-Петербургский политехнический университет Петра Великого,
Санкт-Петербург, Российская Федерация

✉ selin_ia@spbstu.ru

Аннотация. Статья посвящена проблеме эффективного использования энергии на заданном маршруте в гонках солнцемобилей. Солнцемобили это электромобили с возможностью заряда по ходу движения с помощью встроенных солнечных панелей. Гонки солнцемобилей характеризуются очень длинными дистанциями и запретом подзарядки от электросети во время соревнований, болиды могут заряжаться только от солнечной энергии. Это создаёт большой недостаток энергии, а в сочетании с целью соревнований в виде минимизации времени прохождения дистанции, задача ещё больше усложняется. Поэтому критически важно правильно использовать энергию на дистанции. Но оптимизация режимов использования энергии имеет высокую вычислительную сложность, поэтому для ускорения процесса предложено использовать модифицированное представление маршрута и автоматическое дифференцирование. Методы реализованы в программном комплексе SPbPUStrat, способном решать проблему за короткое время, что позволяет перейти к пересчёту стратегии энергопотребления в полном разрешении по запросу.

Ключевые слова: солнцемобиль, стратегия, стратегия использования энергии, оптимизация, представление маршрута

Для цитирования: Selin I.A. New methods for efficient energy management of a solar vehicle on a fixed route // Computing, Telecommunications and Control. 2023. Т. 16, № 4. С. 18–27. DOI: 10.18721/JCSTCS.16402

Introduction

There are quite a few engineering sports competitions. Often used as a competitive testing ground, they help to develop new approaches for solving real-world problems. One of the sustainability-focused competitions mentioned is the solar car racing. Each participating team must build a compliant solar car and drive it over a specified route in the shortest possible time on a single battery charge. But the task seems to be problematic because race courses usually last thousands of kilometers and charging from the grid is prohibited. Participating vehicles are only allowed to charge using built-in solar panels. The lack of energy contradicts the main goal, to complete the route as fast as possible, and creates the need to use available resources in the most optimal way.

Vehicle models used for optimizing the movement of regular vehicles on the route are not suitable for vehicles using alternative power sources. There is a substantial difference in how those vehicles replenish energy. Unlike conventional cars, which only spend stored energy, solar cars can be recharged from solar panels as they move. The rate at which a solar car obtains energy depends on environmental conditions such as solar radiation and weather [1], making it dependent on both time and location. But energy consumption, as in the case of conventional cars, depends on the profile of the road surface and the movement speed. This discrepancy between the energy expenditure and the replenishment significantly complicates the problem. Energy replenishment can be reduced to an indirect dependence on the movement speed, but only at the cost of generating recurrence relations. Considering the goal of

finishing the race in the shortest possible time, this may lead to some counterintuitive conclusions: at some point in the race, it may be more efficient to go faster with more energy consumption, because the energy gain later will be even greater. That's why usually teams in solar car competitions rely heavily on energy management software for computing efficient power management strategies.

The common approach comes down to building a solar car model and formulating an optimization problem in terms of selecting the best controlling inputs to minimize the travel time over the fixed route while satisfying plausibility conditions. The route is usually represented in discrete form as a series of sections connecting route points, with ideally one section corresponding to one control input in the form of speed. Considering that, the problem takes the following form (1):

$$\begin{gathered} J\left(V_1,\, V_2,\, \ldots V_{N-1}\right) = J\left(V_1,\, V_2,\, \ldots V_{N-1}\right) = \sum_{i=1}^{N-1} \frac{\Delta s_i}{V_i} = t_{finish} \to \min, \\ s.t. 0 \le V_i \le V_{\max}, \\ 0 \le E_i\left(V_1,\, V_2,\, \ldots V_{N-1}\right) \le E_{\max}, \\ i \in \mathbb{N},\ 1 \le i \le N, \end{gathered} \tag{1}$$

where Δs_i is a route section length, V_i is a speed on i-th route segment, E_i is an energy at i-th point of the route, N is the number of route points (with $N-1$ route segments). E_i represents the energy balance and can be identified as follows (2):

$$\begin{gathered} E_i = E_{i-1} + E_{i-1}^{+}\left(V_i\right) - E_{i-1}^{-}\left(V_1,\, V_2,\, \ldots V_{i-1}\right),\ \ 2 \le i \le N, \\ E_1 = E_{\max}, \\ 0 \le E_i \le E_{\max}. \end{gathered} \tag{2}$$

The $0 \le E_i\left(V_1,\, V_2,\, \ldots V_{N-1}\right) \le E_{\max}$ is a nonlinear inequality, so the (1) problem can be classified as a single-criteria problem with nonlinear constraints.

Since the routes in solar car races are of great length, the number of track sections is also very large, which leads to the curse of dimensionality. As a result, the problem is considered to be too big to be solved in a direct form. Existing works resort to either simplifying the problem by reducing its resolution [2–4], or by optimizing only for the short distance in front of the solar car with full resolution [5, 6]. Some of these approaches [2, 5, 6] support the so-called online mode, where the strategy is recalculated on demand. But none of them allows obtaining a solution for the full problem size, let alone it being calculated on request in a short amount of time.

This paper is an extension of the already published research by the authors [7, 8] and is devoted to development of new techniques for effective power management of a solar car with an emphasis on the possibility of recalculating the strategy on demand. Suggested approach introduces notable differences in this process: the use of a modified track representation and the use of automatic differentiation in the solar car model for optimization purposes.

Route representation

Route data is introduced as an irregularly discrete set of points with the following information: latitude, longitude and altitude. Lateral data is not needed, since "the lateral vehicle dynamics is omitted in simulations" [2], thus the latitude and longitude are converted into the distance from the start of the race to the point of interest. This is the most common representation and is usually shown on graphs as altitude versus distance (route profile). Next, the data is processed to obtain a representation convenient for modeling purposes: sections between the route points. These segments contain such information as:

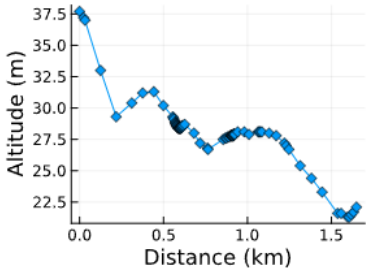

Fig. 1. Route profile

distance between points, elevation difference and inclination angle, calculated based on the original data [3]. Route representation is shown on Fig. 1.

The problem is that routes are very long and contain a very large number of segments, which does not contribute to the complexity of the optimization process. Knowing this, existing approaches work with fairly sparse route data, where one segment corresponds to a route length of more than 5 kilometers [5], which may be sufficient for tracks with a low elevation profile, but not for tracks with high altitude variance. In the literature on solar-powered auto racing, the question of choosing the discreteness of the track has not yet been raised. Therefore, a modified track representation is needed that is as small as possible in terms of the number of segments while still providing adequate simulation results.

Two track data processing techniques are proposed, based on merging neighboring segments with recalculation of their characteristics: keeping only elevation extremum points and parametric segments merge based on the difference in inclination. Both methods consist of 2 stages: selecting track points to keep (points of interest, POI) and then recalculating segment characteristics based on the selected points. Methods are inspired by Zhang S., et. al [9], but for the stated altitude over distance route representation.

When using the extremum point method, only points that are either above neighboring or below neighboring ones, or on the edges of plateau sections are saved in the POI list.

The parametric comparison is based on the slope angle since it is a normalized measure independent of the distance of each segment, which is vital for irregular grid representation. If the difference in a slope angle between adjacent track sections is less than a threshold value (k), then the shared point between the segments is added to the POI list. Threshold value of $k = 0$ will yield original track representation.

After the POI list is formed, the characteristics of new the segments are recalculated to obtain new values for the inclination angle and altitude. Instead of using only the information from the POI to construct the new segments, we are suggesting recalculating the new segments data using all the information so that the characteristics of newly formed combined segments are the same, as if we had simply taken unprocessed segments between the same points.

In the usual building of track segments, characteristics such as latitude, longitude and altitude can be obtained by simple averaging between the edge points of the segment (3):

$$avg = \frac{\mathrm{alt}\left(x_{i+1}\right) + \mathrm{alt}\left(x_i\right)}{2}. \tag{3}$$

But since the merger occurs on an uneven distance grid between the new POIs, there may be different altitude profiles with different average values, while having same altitude at POI. As a result, simply averaging data across POIs will produce wrong results. An example of this can be seen in Fig. 2, where the POIs are located at distances 1 and 4, and depending on the altitude profile, the true average value will be different compared to simple averaging by POI's altitude, which will always yield 4 as a result.

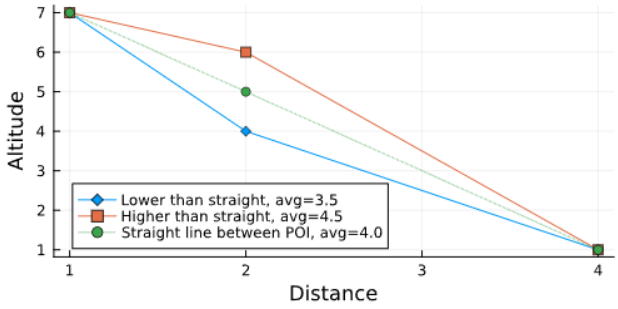

Fig. 2. Averages between POIs

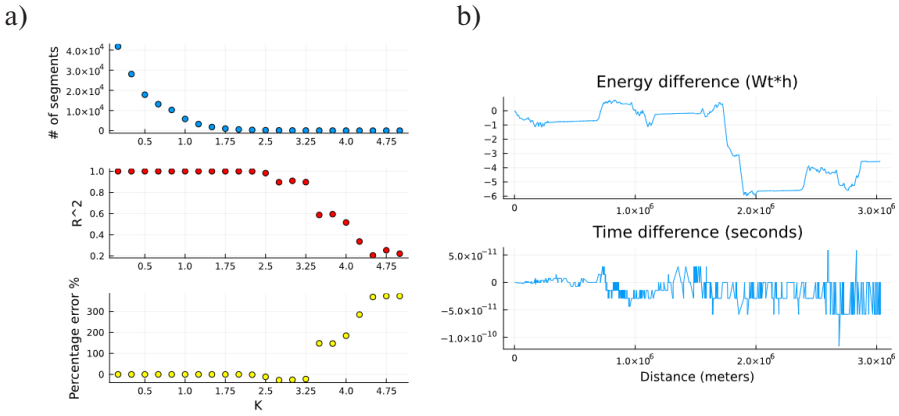

Fig. 3. Modeling quality with different parametric track representation

To avoid this effect, we suggest to perform numerical integration using the trapezoid rule and then average over the distance between the POIs (4):

$$avg = \sum_{i=1}^{k} \left[\frac{\mathrm{alt}(x_{i+1}) + \mathrm{alt}(x_i)}{2} \times (x_{i+1} - x_i) \right] \Big/ (x_k - x_1). \quad (4)$$

It is easy to see that in the case of the usual construction of segments without extracting POI, result will be the same as in (3), since k is equal to 2 and only one sum will be taken, so $(x_k - x_1)$ term cancels. But if multiple segments need to be merged, this will provide true average value, which will give almost the same result when using the processed segments in the model as the original track representation.

Keeping only extremum points as POI allows to reduce the number of segments by approximately 3 times. Parametric variation produces a wide range of results depending on the threshold value (Fig. 3, a). It is clearly seen that there is a certain interval of threshold values (k from 1 to 2.25), where the number of segments is greatly reduced, but the quality of the modeling does not suffer. An example of accumulated simulation error for $k = 1.75$ can be seen on Fig. 3, b. An energy difference of 5 W*h at the finish line is considered negligible, since it is less than 0.1% of the total capacity of the battery and is insignificant compared to the total energy consumption over the whole distance.

A numerical experiment was carried out, where the optimization process was carried out for the given problem (1) on routes of different lengths and different representations. Route representations used: unprocessed, the extrema method, the parametric method with $k = 1.75$. Optimization time and target

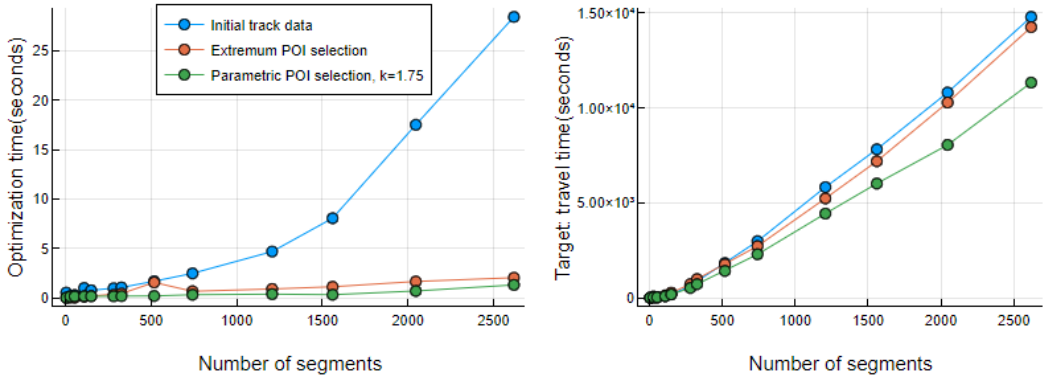

Fig. 4. Optimization and target time

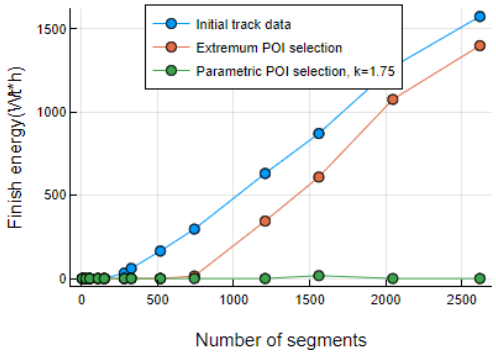

Fig. 5. Energy at the finish line

value (travel time) were measured. Fig. 4 shows that the developed methods show both better performance and achieve better target values.

It is worth noting, that the optimization process does not converge on the original track representation after reaching a problem size of 250 route segments, and after reaching 750 segments for the extrema method. The optimization process converges on routes of all sizes when using the parametric method. Convergence can be determined by the energy value at the finish line, it should be equal to zero. Otherwise, the solution is not optimal. A graph of the amount of energy at the finish is shown in Fig. 5.

Both the parametric method and the extrema method of simplifying the route representation make it possible to reduce the number of sections on the route without significant loss of quality, which leads to an improvement in both the performance and the convergence of the optimization process.

Automatic differentiation

Although the solar car model itself has already been described in the literature [10, 11], its implementation may differ in many ways. Ultimately, the model is built for use in the optimization process. And since optimization requires a lot of resources, its performance should be increased as much as possible.

Gradient-free optimization methods such as Nelder-Mead [12] or evolutionary strategies [13] are commonly used. The literature also describes the use of such 1st order methods as BFGS [14], but only using numerical differentiation, which is fraught with errors and requires additional function calls. However, literature review revealed no use of automatic differentiation in solar car models. Automatic differentiation [15–19] (AD, or differentiable programming) is a technique for automated building of a derivative of a program function, that operates with source code and overloads mathematical functions

and operators with their derivative counterparts. AD allows to program only the original function and to get derivative version of that function automatically, which will yield the same result as in analytical (symbolical) differentiation. But to execute AD, it is necessary to comply with some restrictions on the code of the target function: it must be unary and must not call code written in another language, and must use a certain hierarchy of data types.

Using automatic differentiation in the model allows to generate functions that calculate gradients and Hessians. And having them, it will be possible to apply 1st and 2nd order optimization methods without using numerical differentiation, which will lead to faster convergence.

Our model was adapted to use the automatic differentiation. A computational experiment was carried out to optimize the stated problem using 0th and 1st order methods on problems of different sizes. Both optimization time and target values were recorded. Methods requiring gradients were tested using numerical differentiation (ND) and automatic differentiation (AD). The optimization problem was solved by using methods: Nelder-Mead [12], BFGS [14] and Conjugate gradient [20]. Results can be seen in Table 1. It is clearly seen that 1st order methods using automatic differentiation give both the best result and the best optimization time.

Table 1

Optimization of the stated problem with and without the use of automatic differentiation

Problem size (segments)	Nelder-Mead	BFGS with ND	BFGS with AD	Conjugate gradient with ND	Conjugate gradient with AD
Optimization time (seconds)					
25	0.378	0.100	0.006	0.204	0.363
75	32.726	0.546	0.084	0.023	0.099
150	62.609	0.457	0.152	1.608	0.169
300	159.439	32.641	0.832	1.418	0.625
500	531.791	19.581	3.160	208.245	2.000
Target: travel time (seconds)					
25	356.857	356.810	356.810	356.810	356.810
75	1992.816	1756.572	1676.040	1643.247	1578.299
150	4084.410	3756.140	3642.381	3504.665	3508.342
300	9526.859	8869.733	9020.479	7827.724	7870.441
500	16977.256	14209.110	14636.160	14037.576	13905.262

Software implementation

A typical technology stack for implementing software that includes modeling and optimization will require a variety of tools and technologies. Implementation of the model requires tools with appropriate capabilities (e.g., Modelica, GPSS, SimPy, Simulink), formulation of the optimization problem requires an algebraic modeling language (e.g., AMPL, GAMS, Gekko) connected to the solver, and the application software is developed using a general-purpose language. This results in redundant integration code with additional performance overhead and possible errors. Using a multi-paradigm programming language can help smooth out the corners and get all the necessary steps done.

Our software solution, called SPbPUStrat, is developed using the Julia programming language [21], which is a multi-paradigm language for scientific computing. The solar car and environment models are made in pure Julia and adapted to use automatic differentiation with ForwardDiff.jl package [22]. Optimization problem statement and optimization itself were performed using Optim.jl [23] with

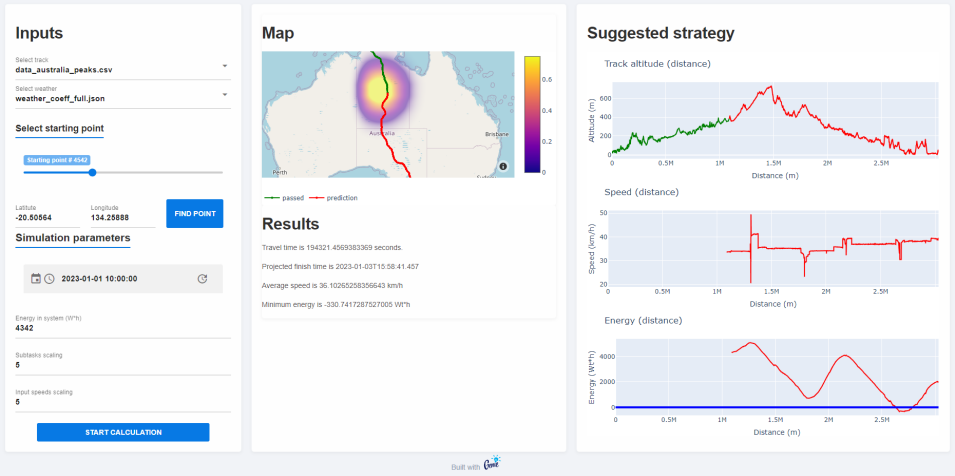

Fig. 6. Strategy dashboard

interior point Newton method [24]. The applied software was created using the Genie framework [25]. Additional packages include CSV.jl [26], Dataframes.jl [27] and Distributions.jl [28]. Thanks to a unified ecosystem, development time was significantly reduced, and almost no integration code was written. It also made debugging much easier and streamlined the delivery process.

The developed software is a client-server solution built according to the MVVM pattern. The software consists of two modules: calculation module and dashboard project. Calculation module provides all the necessary methods for setting the optimization problem and getting the solution. Dashboard module provides the user interaction. User interface can be seen on Fig. 6.

Results and discussion

The use of automatic differentiation and simplified track representation in combination with earlier results were tested by calculating the power management strategy on the full problem size. For comparison purposes, naïve approach (one speed for the entire route) and common approach (reduced problem resolution, 50 inputs) approaches were also tested. The power management strategy was calculated for the case of weather disturbances in the middle of the journey, which significantly affects the energy supplies. The results can be seen in Table 2. Tests were performed on a following configuration: AMD Ryzen 9 5900X, 64GB RAM, Windows 10, Julia 1.9.4 x64.

Table 2

Overall performance and quality results

Approach	Finish time	Improvement (hours)	Calculation time (seconds)	Energy at the finish line (Wt*h)	Scale
Naive	6d 05:17:01	–17.56	0.53	14683.0	Minimal (1)
Common	5d 11:42:68	0.00	14.4	1225.3	Reduced (50)
Proposed	5d 04:54:47	6.81	35.7	15.2	Full (10k+)

The naïve approach does not work well with weather disturbance. The speed has to be reduced to very low values to comply with energy constraints, resulting in much later completion times. The common approach does solve the weather problem and gives a better solution in terms of time. But it is clear that the solution is not optimal and there is a room for improvement, since the energy at the finish line is

above zero. The proposed methods provide a solution where the target value is 6.81 hours faster than the common approach, energy at the end is almost depleted.

Although the running time of the proposed methods is longer than that of other solutions, this is not a critical drawback. Typically, a recalculation of the power management strategy is necessary when the execution of the strategy begins to deviate from the original plan or when environmental conditions have changed, constant recalculation is unnecessary. The performance of the proposed methods is sufficient to perform calculations on request.

Conclusion

The problem of developing software for efficiently managing the energy of a solar car on a fixed route for racing is considered. The advantages and disadvantages of existing approaches were discussed. Opportunities for improvement were found in two areas: route presentation and automatic differentiation. The modified route representation made it possible to reduce the number of segments by up to 10 times without a huge loss in modeling quality. Automatic differentiation in the solar car model enabled the use of higher order optimization, resulting in better performance and convergence.

The proposed methods were implemented in the SPbPUStrat software solution, which allows the end user to recalculate the strategy on the fly during the race: this significantly improves strategic capabilities and increases the chances of success.

REFERENCES

1. **Teshima Y., Hirakoso N., Shigematsu Y., Hirama Y., Kawabata H.** Optimal Driving Strategy for Solar Electric Vehicle, IEEJ Journal of Industry Applications. 2021, Vol. 10, No. 3, Pp. 303–309.

2. **Yesil E., Onol A.O., Icke A., Atabay O.** Strategy optimization of a solar car for a long-distance race using Big Bang – Big Crunch optimization, 2013 IEEE 14th International Symposium on Computational Intelligence and Informatics (CINTI). 2013, Pp. 521–526.

3. **Schoeman S., Carroll J.** A combined energy system model for solar racers, 2013 Africon. Pointe-Aux-Piments, Mauritius: IEEE, 2013, Pp. 1–5.

4. **Wright G.S.** Optimal energy management for solar car race, Proceedings of the 39th Midwest Symposium on Circuits and Systems. 1996, Vol. 3, Pp. 1011–1014.

5. **Mocking C.** Optimal design and strategy for the SolUTra, MSc Report. 2006, Pp. 1–134.

6. **Guerrero Merino E., Duarte-Mermoud M.A.** Online energy management for a solar car using pseudospectral methods for optimal control, Optimal Control Applications and Methods. 2016, Vol. 37, No. 3, Pp. 537–555.

7. **Selin I.A., Kasatkin I.I., Zakhlebaev E.A., Hemminger O.P.** Building a time-optimal power consumption strategy for a solar car, IOP Conference Series: Material Science and Engineering. 2019, Vol. 643, No. 1. P. 012004.

8. **Selin I.A.** Otsenivaniye i optimizatsiya strategii energosberezheniya dlya solntsemobilya [Evaluation and optimization of the energy saving strategy for the solar vehicle], Materials of the XII Multi-conference on Management Problems (ICPU-2019), Southern Federal University Press. 2019. Vol. 2. Pp. 213–216.

9. **Zhang S., Liu K., Yao J.** A Simplified Approach to DEM Based on Important Points and the Triangular Irregular Network Angles, 2023 IEEE 3rd International Conference on Electronic Technology, Communication and Information (ICETCI). 2023, Pp. 934–93.

10. **Pudney P.** Optimal energy management for solar-powered CARS. University of South Australia, 2000.

11. **Thacher E.F.** A Solar Car Primer: A Guide to the Design and Construction of Solar-Powered Racing Vehicles. Cham: Springer International Publishing, 2015.

12. **Nelder J.A., Mead R.** A Simplex Method for Function Minimization, Comput. J. 1965. Vol. 7, No. 4. Pp. 308–313.

13. **Erol O.K., Eksin I.** A new optimization method: Big Bang–Big Crunch, Adv. Eng. Softw. 2006. Vol. 37, No. 2. Pp. 106–111.

14. **Broyden C.G.** The Convergence of a Class of Double-rank Minimization Algorithms 1. General Considerations, IMA J. Appl. Math. 1970. Vol. 6, No. 1. Pp. 76–90.

15. **Ayda-Zade K.R., Yevtushenko Yu.G.** Bystroye avtomaticheskoye differentsirovaniye na EVM [Fast automatic differentiation on a computer]. Matematicheskoye modelirovaniye [Mathematical modeling], 1989, Vol. 1, No. 1. Pp. 120–131.

16. **Zasukhina E.S.** Fast automatic differentiation as applied to the computation of second derivatives of composite functions, Comput. Math. Math. Phys. 2006. Vol. 46, No. 11. Pp. 1835–1859.

17. **Evtushenko Y.** Computation of exact gradients in distributed dynamic systems, Optim. Methods Softw. Taylor & Francis, 1998. Vol. 9, No. 1–3. Pp. 45–75.

18. **Wengert R.E.** A simple automatic derivative evaluation program, Commun. ACM. 1964. Vol. 7, No. 8. Pp. 463–464.

19. **Linnainmaa S.** Taylor expansion of the accumulated rounding error, BIT Numer. Math. 1976. Vol. 16, No. 2. Pp. 146–160.

20. **Hestenes M.R., Stiefel E.** Methods of conjugate gradients for solving linear systems, J. Res. Natl. Bur. Stand. 1952. Vol. 49, No. 6. Pp. 409.

21. **Bezanson J., Edelman A., Karpinski S., Shah Viral B.** Julia: A Fresh Approach to Numerical Computing, SIAM Rev. 2017. Vol. 59, No. 1. Pp. 65–98.

22. **Revels J., Lubin M., Papamarkou T.** Forward-Mode Automatic Differentiation in Julia: arXiv:1607.07892. arXiv, 2016.

23. **Mogensen P.K., Riseth A.N.** Optim: A mathematical optimization package for Julia, J. Open Source Softw. 2018. Vol. 3, No. 24. Pp. 615.

24. **Wächter A., Biegler L.T.** On the implementation of an interior-point filter line-search algorithm for large-scale nonlinear programming, Math. Program. 2006. Vol. 106, No. 1. Pp. 25–57.

25. Genie Framework – Productive Web Development With Julia. Available at: https://genieframework.com/ (accessed: 26.11.2023).

26. **Quinn J. et al.** JuliaData/CSV.jl: v0.10.11. Zenodo, 2023.

27. **Bouchet-Valat M., Kamiński B.** DataFrames.jl: Flexible and Fast Tabular Data in Julia, J. Stat. Softw. 2023. Vol. 107, No. 4.

28. **Dahua Lin et al.** JuliaStats/Distributions.jl: v0.25.103. Zenodo, 2023.

INFORMATION ABOUT AUTHOR / СВЕДЕНИЯ ОБ АВТОРЕ

Selin Ivan A.
Селин Иван Андреевич
E-mail: selin_ia@spbstu.ru
ORCID: https://orcid.org/0000-0002-8805-5887

Submitted: 30.10.2023; Approved: 18.12.2023; Accepted: 21.12.2023.
Поступила: 30.10.2023; Одобрена: 18.12.2023; Принята: 21.12.2023.

Computing, Telecommunication and Control, 2023, Vol. 16, No. 4, Pp. 28–36.
Информатика, телекоммуникации и управление. 2023. Том 16, № 4. С. 28–36.

Simulations of Computer, Telecommunications, Control and Social Systems

Моделирование вычислительных, телекоммуникационных, управляющих и социально-экономических систем

Research article
DOI: https://doi.org/10.18721/JCSTCS.16403
UDC 621.36

CONTACT RESISTANCES INFLUENCE ON FLEXIBLE THERMOELECTRIC GENERATOR OUTPUT POWER

V.V. Loboda ✉

Peter the Great St. Petersburg Polytechnic University,
St. Petersburg, Russian Federation

✉ vera_loboda@mail.ru

Abstract. The calculation results of the influence of contact resistances of the metal-semiconductor interface on the output power of a flexible microthermoelectric generator is presented. The calculation method based on semiconductor theory. The contact area of the conductor (metal) and thermoelectric material (semiconductor) is characterized by a discrepancy between bulk properties and irregularities in a thin area near the interface. Different thermal and electrical carriers (phonons and electrons) encounter different resistances in this interface area. The calculations were carried out using ANSYS Workbench and Wolfram Mathematica. Output power simulation was carried out by taking into account contact electric and thermal resistances influence on the metal–semiconductor interface for six contact couples (three metals, two semiconductors). Interface contact resistances significantly reduce the output power. It was shown that contact resistances reduce the output power of the thermoelectric device by 64–70% depending on the metal type of the metal–semiconductor contact couple. The presented results of calculating interface contact resistances correspond to experimental measurements in references, which allows us to conclude that this method of calculating interface electrical and thermal contact resistances can be used in the case of microelectronic fabrication of thermoelectric devices.

Keywords: thermoelectric generator, contact resistances, simulation, ANSYS, output power

Aknolegement: This work was funded by State Assignment for Basic Research (project FSEG-2023-0016).

Citation: Loboda V.V. Contact resistances influence on flexible thermoelectric generator output power. Computing, Telecommunications and Control, 2023, Vol. 16, No. 4, Pp. 28–36. DOI: 10.18721/JCSTCS.16403

Научная статья
DOI: https://doi.org/10.18721/JCSTCS.16403
УДК 004.67

ВЛИЯНИЕ КОНТАКТНЫХ СОПРОТИВЛЕНИЙ НА ВЫХОДНУЮ МОЩНОСТЬ ГИБКОГО ТЕРМОЭЛЕКТРИЧЕСКОГО ГЕНЕРАТОРА

В.В. Лобода ✉

Санкт-Петербургский политехнический университет Петра Великого,
Санкт-Петербург, Российская Федерация

✉ vera_loboda@mail.ru

Аннотация. Представлены результаты расчета влияния контактных сопротивлений на границе раздела металл-полупроводник на выходную мощность гибкого микротермоэлектрического генератора. Метод расчета основан на теории полупроводников. Область контакта проводника (металла) и термоэлектрического материала (полупроводника) характеризуется несоответствием объемных свойств и неоднородностями в тонкой области вблизи границы раздела. Различные тепловые и электрические носители (фононы и электроны) будут встречать разное сопротивление в этой области интерфейса. Расчеты проводились с использованием программного обеспечения ANSYS Workbench и Wolfram Mathematica. Моделирование выходной мощности проведено с учетом влияния контактных электрических и термических сопротивлений на границу раздела металл-полупроводник для шести контактных пар (три металла, два полупроводника). Контактные сопротивления интерфейса существенно снижают выходную мощность. Показано, что контактные сопротивления снижают выходную мощность термоэлектрического устройства на 64–70% в зависимости от типа металла контактной пары «металл-полупроводник». Представленные результаты расчета интерфейсных контактных сопротивлений соответствуют экспериментальным измерениям в литературе, что позволяет сделать вывод о возможности использования данного метода расчета интерфейсных электрических и тепловых контактных сопротивлений при микроэлектронном изготовлении термоэлектрических устройств.

Ключевые слова: термоэлектрический генератор, контактные сопротивления, моделирование, ANSYS, выходная мощность

Финансирование: Работа выполнена в рамках Государственного задания на проведение фундаментальных исследований (код темы FSEG-2023-0016).

Для цитирования: Loboda V.V. Contact resistances influence on flexible thermoelectric generator output power // Computing, Telecommunications and Control. 2023. Т. 16, № 4. С. 28–36. DOI: 10.18721/JCSTCS.16403

Introduction

There are numerous power sources for low power consumption applications, but there exists a need to design improved alternative sources, and provide reliable and stable power supplies for microelectronic devices such as wireless sensor networks, smart homes, objects monitoring and mobile devices [1, 2]. Lately, the majority of research study on thermoelectric generators (TEG) has focused on volume and thin-film devices based on inorganic thermoelectric materials [3, 4]. One of the most promising types of TEGs that combine properties of inorganic thin-film semiconductor materials and an organic base is flexible microthermoelectric generators [5–7]. Thermoelectric devices design requires considering numerous factors related to the combination of different materials, the main of which are electric and thermal contact resistances. A great amount of research focuses on the influence of resistances on the metal–semiconductor interface [7–16]. Theoretical and experimental methods to measure resistances values are used. The values from the references range for electric contact resistances 10^{-14}–10^{-7} Ohm·m^2

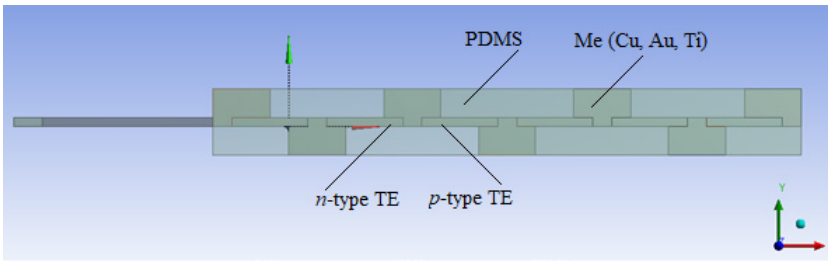

Fig. 1. 3D geometric model of Y-structure microthermoelectric generator

for thermal contact resistances: 10^{-10}–10^{-6} K / (W / m^2). It may be concluded from the references analysis results that application of this or that calculation method or measurements of contact resistances depends directly on semiconductor materials synthesis technology and device design.

The research goal is calculating contact resistance on the metal–semiconductor interface and determining their influence on output characteristics of a flexible microthermoelectric generator.

Contact resistances calculation method

A flexible Y-structure microthermoelectric generator was chosen as the object of the study [17, 18]. It consists of twenty-four *n*- and *p*-type thermoelements (TE) based on solid solutions Bi_2Te_3 and Sb_2Te_3 with contact conductors located between them. Fig. 1 shows a geometric 3D model of a flexible micro TEG. The TE have dimensions of 800 mm × 600 mm × 100 mm, metal contact connections are 600 mm × 600 mm × 300 mm. The rest of the TEG area is filled with a flexible substrate. Linear polymer polydimethylsiloxane (PDMS) is used as the flexible base. The total surface area of the device (S) was 26 mm^2.

The total internal electrical resistance of the TEG can be represented as the sum of series-connected resistors:

$$R_{\text{int}} = \sum_{i=1}^{2N} R_{\text{me}} + R_{\text{cont}},$$

where $R_{(n,\,p)}$ – TE resistance; R_{me} – resistance of metal; R_{cont} – contact resistance on the metal–semiconductor interface.

The internal resistance of the generator and, therefore, the maximum output power depends on the volume of the contact resistance [19].

The contact area of the conductor (metal) and thermoelectric material (semiconductor) is characterized by a discrepancy between bulk properties and irregularities in a thin area near the interface. Different thermal and electrical carriers (phonons and electrons) encounter different resistances in this interface area, resulting in lower power output from the device. The total thermal interface resistance is a circuit of parallel-connected resistances $(A_kR_k)_b$ is defined as [8]:

$$\frac{1}{(A_kR_k)_b} = \frac{1}{(A_kR_k)_{b,pp}} + \frac{1}{(A_kR_k)_{b,ee}} + \frac{1}{(A_kR_k)_{b,ep}} + \frac{1}{(A_kR_k)_{b,pe}}, \quad (1)$$

where A_k – TE cross-section area; R_k – thermal resistance; $(A_kR_k)_{b,pp}$ – phonon resistance; $(A_kR_k)_{b,ee}$ – electron resistance; $(A_kR_k)_{b,ep}$, $(A_kR_k)_{b,pe}$ – electron-phonon resistance. It is assumed that there is no direct heat transfer between the electron and phonon subsystems through the interface.

To calculate the phonon resistances, the diffuse mismatch model [8] is used, in which it is assumed that all phonons falling on the interface scatter.

The phonons boundary resistance may be calculated by the equation:

$$\frac{1}{\left(A_{\mathrm{k}}R_{\mathrm{k}}\right)_{\mathrm{b,pp}}}=\frac{T_{\mathrm{te}}-T_{\mathrm{mc}}}{q}, \tag{2}$$

where q – heat flux caused by an increase in the semiconductor temperature T_{te} relative to the substrate temperature T_{mc}.

The expression for the heat flux as a function of the phonon density of states may be represented starting from the general expression for the energy transferred per unit time from the semiconductor to the metal. Assuming that the transfer coefficient does not depend on the temperature on either side of the interface (only one side of the interface is considered):

$$q=\frac{h_{\mathrm{P}}\tau_{\mathrm{te}\to\mathrm{mc}}}{8\pi}\sum\nolimits_j U_{p(\mathrm{te},j)}\int_0^{\infty}P_{p,D}\left(\omega_p\right)\omega_p\left[\frac{1}{\exp\left(\dfrac{h_{\mathrm{P}}\omega_p}{2\pi k_{\mathrm{B}}T_{\mathrm{te}}}\right)}-\frac{1}{\exp\left(\dfrac{h_{\mathrm{P}}\omega_p}{2\pi k_{\mathrm{B}}T_{\mathrm{mc}}}\right)}\right]d\omega_p, \tag{3}$$

where h_{P} – Planck's constant; $\tau_{\mathrm{te}\to\mathrm{mc}}$ – heat transfer coefficient; $U_{p(\mathrm{te},j)}$ – the velocities of phonon modes in a semiconductor; $P_{p,D}$ – phonon states density; ω_p – angular frequency; k_{B} – Boltzmann's constant.

The phonon wave velocities (two transverse and one longitudinal) are calculated by the equation:

$$\sum\nolimits_j\frac{1}{U_{p(\mathrm{te},j)}}=\frac{1}{U_{p(\mathrm{te},l)}}+\frac{1}{U_{p(\mathrm{te},t)}}. \tag{4}$$

The transmission coefficient is approximated by the equation:

$$\tau_{\mathrm{te}\to\mathrm{mc}}=\frac{\sum_j u_{p(\mathrm{mc},j)}^{-2}}{\sum_j u_{p(\mathrm{te},j)}^{-2}+u_{p(\mathrm{mc},j)}^{-2}}. \tag{5}$$

Equation (5) is derived for the case when T_{te} equals T_{mc}, i.e. the equation gives a sufficient prediction of the transmission coefficient for a small $T_{\mathrm{te}}-T_{\mathrm{mc}}$. Usually, this temperature difference is about 1 K, which will be used in calculations.

The phonon velocity and Debye temperature are related to the Debye angular frequency ω_{D} through the equations:

$$\omega_{\mathrm{D}}=\left(6\pi^2u_p^3n\right)^{\frac{1}{3}}, \tag{6}$$

$$T_{\mathrm{D}}=\frac{h_{\mathrm{P}}\omega_{\mathrm{D}}}{2\pi k_{\mathrm{B}}}, \tag{7}$$

where n – the ratio of the number of primitive cells to the volume of a unit cell. Bi_2Te_3 and Sb_2Te_3 have non-primitive hexagonal unit cells three times the volume of a primitive rhombohedral cell [1].

The Debye density of phonon states is defined as:

$$P_{p,D}=\frac{\omega_p^2}{2\pi^2u_p^3}, \tag{8}$$

The boundary resistance of electrons was determined by the equation:

$$\frac{1}{\left(A_{\mathrm{k}}R_{\mathrm{k}}\right)_{\mathrm{b,ee}}}=\frac{\pi^2}{3}\frac{T}{\left(A_{\mathrm{k}}R_{\mathrm{e}}\right)_{\mathrm{b}}}\left(\frac{k_{\mathrm{B}}}{e_c}\right)^2, \tag{9}$$

where $(A_{\mathrm{k}}R_{\mathrm{e}})_{\mathrm{b}}$ – electrical interface resistance:

$$\frac{1}{\left(A_{\mathrm{k}}R_{\mathrm{e}}\right)_{\mathrm{b}}}=\frac{4\pi e^2 m_{\mathrm{e,te}}P}{h_P^3}\left[\frac{h_P^2E_0}{8\pi^2 m_{\mathrm{e,te}}d^2}\right]^{\frac{1}{2}}, \tag{10}$$

where $m_{\mathrm{e,te}}$ – effective mass of electrons/holes in thermoelectric material; e – electron charge; P – tunneling probability; E_0 – potential barrier height, d – potential barrier thickness.

The electrical contact resistance is calculated by the equation:

$$R_{\mathrm{e,c}}=\frac{4N_{\mathrm{te}}\left(A_{\mathrm{k}}R_{\mathrm{e}}\right)_{\mathrm{c}}}{A_{\mathrm{k}}}, \tag{11}$$

where N_{te} – number of thermoelements.

Table 1 displays the numerical values of the parameters of thermoelectric materials for calculating the thermal contact resistance.

Table 1

The parameters of thermoelectric materials [8]

Parameter	**Bi_2Te_3**	**Sb_2Te_3**
n, m^{-3}	$5.95\cdot10^{27}$	$6.40\cdot10^{27}$
ω_D, $rad\cdot s^{-1}$	$2.16\cdot10^{13}$	$2.09\cdot10^{13}$
u_p, $m\cdot s^{-1}$	3.058	2.888
$\tau_{\mathrm{te}\rightarrow\mathrm{mc}}$	0.56	0.54
τ_m, s	$2.5\cdot10^{-14}$	$9.8\cdot10^{-14}$
τ_e, s	$1.0\cdot10^{-11}$	$2.7\cdot10^{-11}$
$m_{\mathrm{e,te}}$	$0.58m_{\mathrm{e,o}}$	$1m_{\mathrm{e,o}}$
E_0, eV	0.15	0.2
d, nm	2.06	2.12

The calculation of contact resistances according to formulas (1–11) was carried out in the Wolfram Mathematica package, the results of calculations at T_{te} = 300 K are presented in Table 2. The solution of the problem of determining the influence of the contact resistance on the flexible micro TEG output power was carried out based on the finite element method using the ANSYS Workbench software platform. The simulation process consists of the following stages as indicated in Fig. 2.

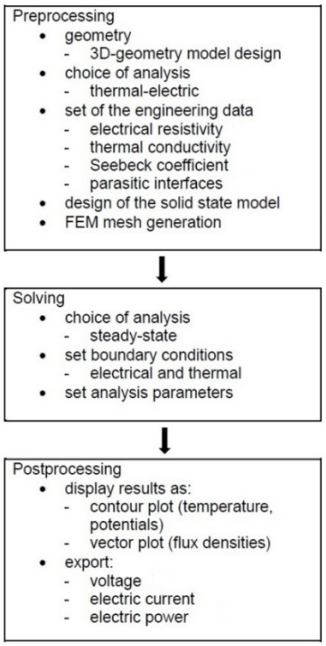

Fig. 2. Simulation process flow-chat

Table 2

Contact resistances calculation results

Thermal interface resistance	**Bi_2Te_3/Metal, K/(W/m²)**	**Sb_2Te_3/Metal, K/(W/m²)**
Phonon, Eq. (2),	$8.7\cdot10^{-8}$	$7.6\cdot10^{-11}$
Electron, Eq. (9)	$3.5\cdot10^{-7}$	$9.7\cdot10^{-7}$
Total, Eq. (1)	$6.9\cdot10^{-8}$	$7.0\cdot10^{-8}$
Electric interface resistance	Bi_2Te_3/Metal, (Ohm·m²)	Sb_2Te_3/Metal, (Ohm·m²)
Cu	$1.8\cdot10^{-8}$	$1.9\cdot10^{-8}$
Au	$2.3\cdot10^{-8}$	$2.5\cdot10^{-8}$
Ti	$3.3\cdot10^{-8}$	$4.1\cdot10^{-8}$

Preprocessing, Solving, Postprocessing. The Preprocessing stage includes five steps: 3-dimensional (3D) model design, choice of the thermal-electric analysis, setting of the engineering data that are physical parameters of materials and their interfaces, design of the solid state model of the thermoelectric generator using ANSYS Mechanical module, and generation of the finite-element mesh by ANSYS Meshing. The Solving stage includes three steps: choice of the steady-state analysis and its options, choice of the electrical and thermal initial conditions, choice of the analysis parameters. The load resistor R_L is modeled using additional APDL (ANSYS Parametric Design Language) procedure. The last stage deals with the output of calculated and simulated results in tables and figures. The simulation procedure is described in detail in [19–22].

Simulation Results

We simulated the output parameters of a flexible microthermoelectric generator for three different contact metals (Cu, Au, Ti) with and without taking into account contact resistances influence.

Bismuth and antimony tellurides of *n*-type and *p*-type conductivity were used as materials for micro-TEG thermoelements, as they provide the maximum thermoelectric efficiency in the considered temperature range. Initial data for simulation include the following physical parameters: Seebeck coefficient, electrical resistivity, thermal conductivity. These parameters largely depend on the semiconductor synthesis technology and have a significant spread. In this concern, the results of processing these parameters by the least-squares method [23] were used as the initial data. Physical parameters of substrate and metal were selected from the ANSYS library. The values of the physical parameters of the components materials of the TEG were used in the simulation for the temperature range of 300–400 K.

The temperature boundary conditions were determined by the temperature of the lower plate T_h and the temperature of the upper plate T_c. We considered the following temperatures: T_h = 318 K, 310 K, 303 K, T_c = 283 K, 280 K, 278 K. These temperatures correspond to the temperature difference between the hot and cold sides ΔT = 25 K, 30 K and 35 K, respectively. As electrical boundary condition, one of the load ports was set to ground (i.e. zero potential).

The results of the simulation are the values of the TEG output power at an external load and the specific power (power on the square unit). The values of the load resistance R_L varied from 0.5 to 30 Ohm. The output voltage was simulated at the load, while the output electric current and power were calculated. The maximum electric output power was calculated assuming that the load resistance was equal to the internal resistance of the generator, i.e. under the condition of transferring maximum electrical power to the load.

The simulation was carried out with and without taking into account the previously calculated contact resistances. The calculation results are presented in Table 3.

Table 3

The maximum output power and specific power of the TEG for various metals

Metal	without contact resistances influence		with contact resistances influence		Δ, %
	P_{max}, μW	P_{max}/S, μW/mm²	P_{max}, μW	P_{max}/S, μW/mm²	
ΔT = 25 K					
Cu	53.8	2.07	19.3	0.74	64
Au	53.8	2.07	19.2	0.74	64
Ti	53.8	2.07	16.3	0.63	70
ΔT = 30 K					
Cu	85.8	3.30	30.3	1.16	65
Au	85.8	3.30	30.2	1.16	65
Ti	85.8	3.30	25.5	0.98	70
ΔT = 35 K					
Cu	133.1	5.12	48.2	1.85	64
Au	133.1	5.12	48.1	1.85	64
Ti	133.1	5.12	40.8	1.57	69

The following results were achieved:

• contact electric and thermal resistances quite strongly influence the output characteristics of the microthermolectric devices, and reduce the output power of a device by 64–70% depending on the metal type of the metal–semiconductor contact couple;

• the greatest contribution to the decrease in output power is produced by the electrical contact resistance at the metal–semiconductor interface;

• the value of electric contact resistance increases in the order of Cu, Au and Ti;

• the value of the thermal contact resistance depends on the type of thermoelectric semiconductor material and does not depend on the choice of the metal of the contact couple.

Conclusions

The presented results of calculating interface contact resistances correspond to experimental measurements [12, 15], which allows us to conclude that this method of calculating interface electrical and thermal contact resistances can be used in the case of microelectronic fabrication of thermoelectric devices. We carried out an output power simulation by taking into account contact electric and thermal resistances influence on the metal–semiconductor interface for six contact couples (three metals, two semiconductors). Interface contact resistances significantly reduce the output power. The presented calculated method makes it possible not only to determine the optimal contact pairs, but also the value of the internal resistance, which in turn makes it possible to develop microelectronic thermoelectric devices, taking into account the operating conditions for power consumption with known external loads.

REFERENCES

1. **Champier D.** Thermoelectric generators: A review of applications, Energy Conversion and Management, 2017, Vol. 140, Pp. 167–181. DOI: 10.1016/J.ENCONMAN.2017.02.070

2. **Rodriguez R., Preindl M., Cotton J.S., Emadi A.** "Review and Trends of Thermoelectric Generator Heat Recovery in Automotive Applications," IEEE Trans. Vehicular Tech., 2019, Vol. 68, No. 6, Pp. 5366–5378. DOI: 10.1109/TVT.2019.2908150

3. **Yan J., Liao X., Yan D., Chen Y.** Review of Micro Thermoelectric Generator, J. Microelectromechanical Syst., 2018, Vol. 27, No. 1, Pp. 1–18. DOI: 10.1109/JMEMS.2017.2782748

4. **Pourkiaei S.M. et. al.** Thermoelectric cooler and thermoelectric generator devices: A review of present and potential applications, modeling and materials, Energy, 2019, Vol. 186, No. 115849, Pp. 1–17. DOI: 10.1016/J.ENERGY.2019.07.179

5. **Deng F., Qiu H., Chen J., Wang L., Wang B.** Wearable Thermoelectric Power Generators Combined With Flexible Supercapacitor for Low-Power Human Diagnosis Devices, IEEE Transactions on Industrial Electronics, 2017, Vol. 64, No. 2, Pp. 1477–1485. DOI: 10.1109/TIE.2016.2613063

6. **Du Y., Xu J., Paul B., Eklund P.** Flexible thermoelectric materials and devices, J. Applied Materials Today, 2018, Vol. 12, Pp. 366–388. DOI: 10.1016/J.APMT.2018.07.004

7. **Wang Y. et al.** Flexible Thermoelectric Materials and Generators: Challenges and Innovations, J. Advanced Materials, 2019, Vol. 31, Pp. 1807916. DOI: 10.1002/adma.201807916

8. **Da Silva L.W., Kaviany M.** Micro-thermoelectric cooler: interfacial effects on thermal and electrical transport, J. International Journal of Heat and Mass Transfer, 2004, Vol. 47, Pp. 2417–2435. DOI: 10.1016/J.IJHEATMASSTRANSFER.2003.11.024

9. **Kim C.H.** Development of a numerical method for the performance analysis of thermoelectric generators with thermal and electric contact resistance, J. Applied Thermal Engineering, 2018, Vol. 108, Pp. 408–417. DOI: 10.1016/j.applthermaleng.2017.10.158

10. **Chen B. et al.** Flexible thermoelectric generators with inkjet-printed bismuth telluride nan-owires and liquid metal contacts, Nanoscale, 2019, Vol. 11, Pp. 5222–5230. DOI: 10.1039/c8nr09101c

11. **Luo Y., Kim C.H.** Effects of the cross-sectional area ratios and contact resistance on the performance of a cascaded thermoelectric generator, J. International Journal of Energy Research, 2019, Vol. 43, No. 3, Pp. 572–596. DOI: 10.1002/ER.4426

12. **Lahmar A. et al.** Experimental investigation on the thermal contact resistance between gold coating and ceramic substrates, J. Thin Solid Film, 2001, Vol. 389, Pp. 167–172. DOI: 10.1016/S0040-6090(01)00774-X

13. **Sim M., Park H., Kim S.** Modeling and Extraction of Parasitic Thermal Conductance and Intrinsic Model Parameters of Thermoelectric Modules, J. Journal of Electronic Materials, 2015, Vol. 44. No. 11, Pp. 4473–4481. DOI: 10.1007/s11664-015-3985-0

14. **Gao Y. et al.** Nanostructured Interfaces for Thermoelectrics, J. Journal of Electronic Materials, 2010, Vol. 39, Pp. 1456–1462. DOI: 10.1007/S11664-010-1256-7

15. **Gupta R.P., Mccarty R., Sharp J.** Practical Contact Resistance Measurement Method for Bulk Bi2Te3-Based Thermoelectric Devices, J. Journal of Electronic Materials, 2014, Vol. 43, No. 6, Pp. 1608–1612. DOI: 10.1007/s11664-013-2806-6

16. **Hodes M.** Optimal Design of Thermoelectric Refrigerators Embedded in a Thermal Resistance Network, J. IEEE Transactions on Components, Packaging and Manufacturing Technology, 2012, Vol. 2, No. 3, Pp. 483–495. DOI: 10.1109/TCPMT.2011.2166762

17. **Nguyen H.T., Nguyen V.T., Takahito O.** Flexible thermoelectric power generator with Y-type structure using electrochemical deposition process, Applied Energy, 2018, Vol. 210, Pp. 467–476. DOI: 10.1016/J.APENERGY.2017.05.005

18. **Buslaev R., Galitskaya A., Loboda V.** Simulation of Flexible Thermoelectric Generators Based on Bi2Te3/Sb2Te3 Synthesized by Electrochemical Deposition Method, in Proc. IEEE International Conference on Electrical Engineering and Photonics (EExPolytech), 2019, Pp. 54–57.

19. **Korotkov A.S., Loboda V.V.** Thermoelectricity: From History to Modernity through the CASS Activity, IEEE Circuits and Systems Magazine, 2021, Vol. 21, No. 3, Pp. 57–65. DOI: 10.1109/mcas.2021.3092534

20. **Loboda V., Buslaev R.** Optimization Calculation of Thermoelement Linear Dimensions for Microthermoelectric Generator, in Proc. 2020 IEEE East-West Design & Test Symposium (EWDTS), Varna, Bulgaria, 4–7 September 2020. DOI: 10.31114/2078-7707-2020-3-230-236

21. **Buslaev R., Loboda V.** Simulation of Uni-leg Thermoelectric Generator, in Proc. IEEE International Conference on Electrical Engineering and Photonics, (EExPolytech), 2018, Pp. 27–31. DOI: 10.1109/EEXPOLYTECH.2018.8564405

22. **Korotkov A.S., Loboda V.V.** Simulation and Design of Thin-Film Thermoelectric Generators, in Proc. International Symposium on Fundamentals of Electrical Engineering (ISFEE), Bucharest, Romania, 4 pages, 1–3 November, 2018. DOI: 10.1109/ISFEE.2018.8742452

23. **Korotkov A.S., Loboda V.V., Dzyubanenko S.V., Bakulin E.M.** Design of a Thin-Film Thermoelectric Generator for Low-Power Applications, Russian Microelectronics, 2019, Vol. 48, No. 5, Pp. 326–334. DOI: 10.1134/s1063739719040061

INFORMATION ABOUT AUTHOR / СВЕДЕНИЯ ОБ АВТОРЕ

Loboda Vera V.
Лобода Вера Владимировна
E-mail: vera_loboda@mail.ru
ORCID: https://orcid.org/0000-0003-3103-7060

Submitted: 16.11.2023; Approved: 13.12.2023; Accepted: 21.12.2023.
Поступила: 16.11.2023; Одобрена: 13.12.2023; Принята: 21.12.2023.

Computing, Telecommunication and Control, 2023, Vol. 16, No. 4, Pp. 37–48.
Информатика, телекоммуникации и управление. 2023. Том 16, № 4. С. 37–48.

Research article
DOI: https://doi.org/10.18721/JCSTCS.16404
UDC 004.04

OPTIMIZATION AND CONTROL SYSTEM OF POWER CONSUMPTION BASED ON VIRTUAL POWER PLANT TECHNOLOGY

Yu.N. Kozhubaev[1] ✉ , *D.S. Kazanin*[2]

[1] Saint-Petersburg Mining University, St. Petersburg, Russian Federation;
[2] Peter the Great St. Petersburg Polytechnic University, St. Petersburg, Russian Federation

✉ y.n.kozhubaev@gmail.com

Abstract. In modern society, the problem of electricity is becoming more and more acute. Until now, most of the electricity has been produced from non-renewable sources: oil, gas, coal and the like. Moreover, the use of such resources leads to environmental pollution and depletion of the Earth's interior. Despite the lack and finiteness of non-renewable energy resources, we can still face excessive energy production. This problem arises due to the fact that it is impossible to accurately predict in advance the amount of electricity that the consumer will need. This, in turn, entails obtaining a significant amount of unused electricity. The use of virtual power plant technology will help to solve this problem. Nowadays, mobile technologies that allow you to solve important issues and problems from anywhere in the world are becoming increasingly popular. These portable technologies, along with the technology of a virtual power plant, will simplify the control of electricity production and costs.

Keywords: Virtual power plant, Industry 4.0, Internet of Things, energy consumption, renewable energy

Citation: Kozhubaev Yu.N., Kazanin D.S. Optimization and control system of power consumption based on virtual power plant technology. Computing, Telecommunications and Control, 2023, Vol. 16, No. 4, Pp. 37–48. DOI: 10.18721/JCSTCS.16404

Научная статья
DOI: https://doi.org/10.18721/JCSTCS.16404
УДК 004.04

СИСТЕМЫ УПРАВЛЕНИЯ И ОПТИМИЗАЦИИ ЭНЕРГОПОТРЕБЛЕНИЕМ НА БАЗЕ ТЕХНОЛОГИЙ ВИРТУАЛЬНОЙ ЭЛЕКТРОСТАНЦИИ

Ю.Н. Кожубаев[1] ✉ , *Д.С. Казанин*[2]

[1] Санкт-Петербургский горный университет,
Санкт-Петербург, Российская Федерация;

[2] Санкт-Петербургский политехнический университет Петра Великого,
Санкт-Петербург, Российская Федерация

✉ y.n.kozhubaev@gmail.com

Аннотация. В современном обществе всё более остро встаёт проблема электроэнергии. До сих пор большая часть электроэнергии производится за счёт невозобновляемых источников: нефть, газ, уголь и подобных. Более того, использование некоторых подобных ресурсов влечёт за собой загрязнение окружающей среды и истощение недр земли. Несмотря на недостаток и конечность невозобновляемых энергоресурсов, мы до сих пор можем столкнуться с избыточным энергопроизводством. Данная проблема возникает вследствие того, что заранее нельзя точно предсказать объем электроэнергии, который потребуется потребителю. Это, в свою очередь, влечёт за собой получение довольно значительного объема неиспользуемой электроэнергии. Использование технологии виртуальной электростанции позволит помочь с решением данной проблемы. В наше время всё большую популярность получают мобильные технологии, которые позволяют решать важные вопросы и проблемы из любой точки планеты. Данные портативные технологии в сочетании с технологией виртуальной электростанции позволят упростить контроль производства и затрат электроэнергии.

Ключевые слова: Виртуальная электростанция, Индустрия 4.0, Интернет вещей, энергопотребление, возобновляемая энергия

Для цитирования: Kozhubaev Yu.N., Kazanin D.S. Optimization and control system of power consumption based on virtual power plant technology // Computing, Telecommunications and Control. 2023. T. 16, № 4. C. 37–48. DOI: 10.18721/JCSTCS.16404

Introduction

The Fourth Industrial Revolution, also known as the Digital Revolution or Industry 4.0, aims at improving the quality of life for all segments of society by integrating accessible digital technologies into everyone's daily life [1–3].

The digital revolution includes various aspects based on various systems: physical systems (CPS), Internet systems (iOS) and the Internet of Things (IOT) familiar to many [4–6].

This industrial revolution can be characterized by the introduction of more flexible technologies for mass-demand goods, which entailed a transition to a new, qualitatively different level of production automation. In turn, more competent and economical energy consumption and the transition to renewable sources of electricity are also important.

Industry 4.0 covers many areas of scientific, industrial and information activities, such as additive manufacturing, the Internet of Things, cloud computing, modeling and much more.

In general, the mathematical formulation of the optimization problem consists in determining the largest or smallest value of the objective function $f(x1, ..., xn)$ under the conditions $gi\ (x1, ..., xn) \le bi\ (i = 1, ..., m)$,where f and gi are set functions, bi are some real numbers. If all f and gi are linear, then the corre-

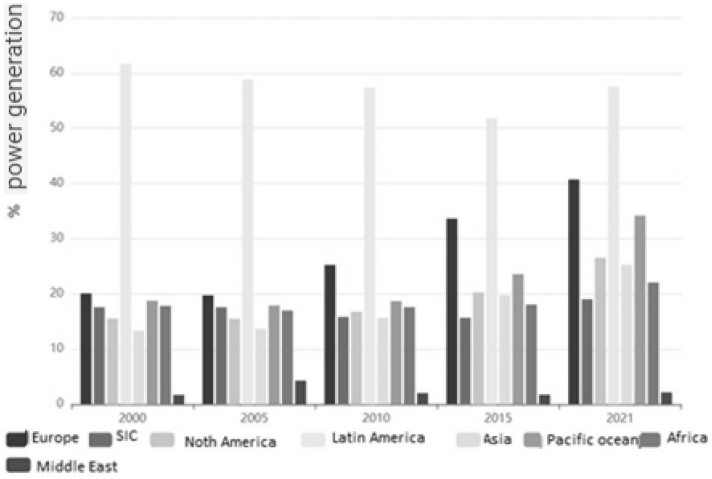

Fig. 1. The trend of renewable energy generation [10]

sponding problem is a linear programming problem. If at least one of these functions is nonlinear, then the corresponding problem is a nonlinear programming problem. Let $z = f(x1, x2, ..., xn)$. Then we can write: z*max (min) and $gi(x1, ..., xn)$ £ bi, $i = 1, ..., m$.

This model can be interpreted as follows to the problems of choosing the best options for economic behavior: z is the optimization goal of the economic system; $f(x1, ..., xn)$ is the corresponding objective function; $x1, x2, ..., xn$ are indicators of the degree of using the means to achieve the goal, which can characterize the output of different types of products, equipment utilization, resource use, etc.

$gi(x1, ..., xn)$ is a function of the total cost of funds of the i-th group used to achieve goals;

bi are the marginal limits of the total cost of funds of the i-th group, are fixed by a restriction on $gi(x)$ above.

The best results are shown by a model using various concepts of the Industry 4.0.

Alternative energy

The main aspect of the Fourth Industrial Revolution is the receipt and proper use of electricity and the transition from non-renewable sources of its production to renewable ones.

Renewable energy or, as it is also called, alternative energy is obtained from natural sources that do not deplete the environment (solar, wind, water, etc.). This type of energy is becoming increasingly popular, because within the framework of Industry 4.0, environmental protection plays an important role if it is necessary to obtain a fairly large amount of electricity [7–9].

In the future, it is assumed that over the next two to three decades, more than two-thirds of the electricity received will be produced from renewable sources.

However, it is worth noting that one of the most important problems is not only obtaining the vast majority of energy resources from renewable sources, but also their competent distribution. This problem arises because of the distance between clean energy sources and the distribution and storage centers of energy resources.

As a solution to this problem, it is possible to introduce a digitized energy network in which all routes of energy resources, places of their shortage and excess will be most transparent. Of course, for a more flexible and accurate management of this network, it would be necessary to involve the consumer in it, but already in the intermediary role in the transfer of energy resources.

Gradually, consumers will be able not only to use and transmit electricity, but also to store, produce, purchase, sale, and manage the course of stored electricity. New scientific developments are already heading in the direction of the most effective ways for users to carry out all these operations [10–12].

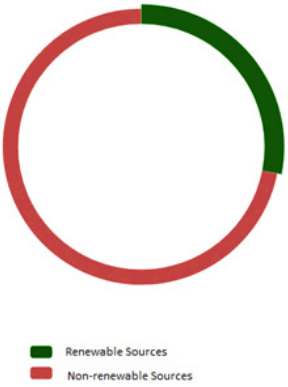

Fig. 2. Share of renewable energy for 2021 [10]

As part of all this, new virtual environment markets and various intelligent platforms will gain even more weight. They will facilitate and accompany the emergence of new business models that allow individuals or different communities to control energy consumption and utilization.

Based on all this, according to forecasts, the formation of an energy system in which the consumer will be able to sell his excess energy will begin by 2030. Within the framework of Industry 4.0, everyone will be able to contribute to the development and change of the entire society and economy.

Using the Internet of Things in the energy sector

The reduction of economic problems to optimization models of solutions, which are a concretization of the general problem of mathematical programming, is based on a number of initial assumptions about the nature of the analyzed economic processes and the choice of the best solutions.

One of these optimization models may be a model for the exchange of excess electricity using the Internet of Things.

The Internet of Things (IoT) is a sector of progressive information technologies, which includes many different aspects.

Various consumer solutions can be attributed to IoT, such as "smart home", intelligent and interactive personal gadgets and various types of intelligent technology. Also, various business and industrial solutions can be attributed to the Internet of Things.

Various devices with their own built-in module or IoT chip are best suited for creating a common network in which various operations will be transmitted in real time. If we add data exchange and two-way communication, we can get a solution for data monitoring and processing, as well as the ability to remotely monitor various operations [13–15].

Smart meters based on IoT can be perceived as intelligent systems for the consumer segment that will help in creating a common network. After all, IoT is a network of physical carriers that have the ability to exchange data. If we apply this concept to utility meters, we will be able to integrate various utility and energy companies into the smart grid that contribute to the distribution, storage and control of energy resources.

Smart meters, which will form the basis of the power grid, will allow utilities to receive and provide complete information about electricity flows. This, in turn, will allow end-users to have better control over their investments in the energy network.

However, this approach requires some solutions from telecommunications and electrical networks. After all, reliable and convenient data transmission technology is necessary for the correct operation of the entire IoT meter infrastructure. For example, it would be quite difficult to use power lines in an intelligent network for communication, even though it is used in Europe. The use of wired telephone networks for

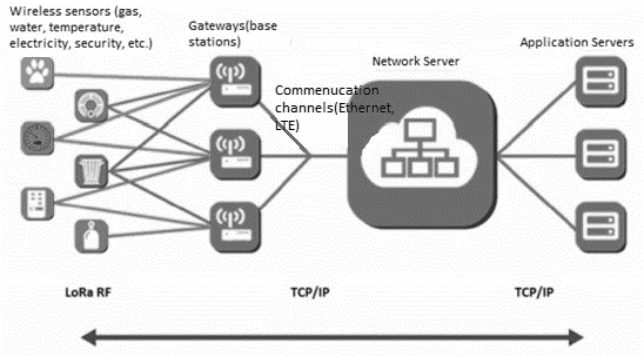

Fig. 3. LoRaWAN

the purpose of transmitting meter data is also often difficult. In this regard, for the counter to work on the IoT platform, a reliable connection is necessary, which cannot always be provided [16–18].

A broadband Wide Area Network (LoRaWAN) can be used as one of the possible solutions to this problem. It was specially designed to support devices on the IoT platform. This modern network solution uses several ISM band frequencies, which depend on the region of application.

Although this technology can only support some specific bandwidth for each device, but this approach is much more deterministic and systematic. For example, meters for the disposal of gas emissions can be mounted independently of the main source of energy supply.

In addition, the service life can reach up to 15 years, thanks to the low power consumption functionality of the LoRaWAN network. The range of such a network can vary from 4 to 20 km, which is a significant advantage for creating a complete infrastructure of meters on this basis.

As an example, one of these networks, which is currently considered the largest LoRaWAN network, is being built by Tata Communications in India. Such a large network on the open IoT platform can be used not only for smart meters, but also as one of the most important components of smart cities [19–21].

The following points can serve as criteria for choosing the Internet of Things for optimization and management:

Cost reduction. The Internet of Things allows you to reduce financial costs when managing energy consumption. Enterprises and individuals reduce energy consumption by controlling and optimizing it using Industry 4.0 concepts. Energy storage technologies and the use of renewable energy sources can help reduce energy consumption.

Improving efficiency. The Internet of Things and cloud solutions can improve energy efficiency by automating energy-intensive processes and optimizing energy consumption. This can help businesses and individuals reduce energy consumption and increase productivity.

Processing large amounts of data. By collecting and analyzing energy consumption data, IoT and cloud solutions enable businesses and individuals to make data-driven energy use decisions. This can help them identify areas where energy is being wasted and make informed decisions about energy use, resulting in cost savings and increased sustainability.

Smart buildings. IoT and cloud-based energy management solutions are also evident in smart buildings. With automation and sensors, smart buildings can optimize energy consumption and reduce costs. Smart building solutions include smart thermostats, lighting, and energy-efficient HVAC systems.

Virtual Power Plant Technologies

Due to the high demand for electricity, there is also a need for clear control over the activities of each power plant. The virtual power plant technology copes with this very well. Virtual power plants are software and hardware complexes that allow managing numerous power generation plants, as if they were a single power plant.

Special software distributes electricity between end users, as well as allows you to store "surpluses" that can be used in the future to compensate for deficiencies during daily production declines. An important and responsible part is precisely the dynamic (and real-time) distribution of power supplies between consumers. This is a rather complex process in which many different factors have to be taken into account: the number of consumers, their relative location (their coordinates), the location of adjacent and responsible energy sources, the parameter of terrain variability and the scale factor. Depending on all this, load centers will be calculated. They are calculated using the method of potential functions and the formula:

$$\prod(x,y) = \sum_{(i=1)}^{n} \left[P_i * e^{-a*\left[(x-x_i)^2+(y-y_i)^2\right]} \right], \quad (1)$$

where n is the number of consumers; x and y are the coordinates of these consumers; P is the power of the consumer; and a is the parameter of terrain variability.

The extremes of this function will be the optimal locations of power sources. In turn, consumers are divided into groups corresponding to the coordinates of power sources. The distribution is made according to the formulas:

$$x_i = \frac{X * P_i}{\sum_k (P_i)_k}, \quad (2)$$

$$y_i = \frac{Y * P_i}{\sum_k (P_i)_k}, \quad (3)$$

where X and Y are the coordinate vectors of consumers of the i-th group; P_i is the power vector of consumers of the i-th groupv; and k is the group number.

Another important aspect of such software is the presence of self-learning artificial intelligence, which allows you to predict production declines and excessive peaks in advance. By optimizing traffic within a single power grid, such software allows you to smooth out unnecessary deviations, which, in turn, has a positive effect on the performance of the entire power grid. As the power grid can include such units as various energy producers (solar power plants, thermal power plants, hydroelectric power plants), virtual power plants, therefore, figuratively speaking, there can be an exchange between sellers and buyers of electricity [22–24].

One of the goals of the virtual power plant is the possibility of joint energy trading and the flexibility to manipulate the production of this very energy. In turn, any decentralized unit for the production, consumption or exchange of electricity can be integrated into the public network of a Virtual Power Plant.

This system structure includes:

1. Energy producer
2. The consumer
3. Accumulators for energy storage
4. VoIP gateways
5. Software for managing the overall operation of the network

Since virtual power plants consist of network assets that produce energy from alternative (renewable) sources, the total capacity of such a station can constantly change. In order to reduce fluctuations in the production capacity, assets of a different nature of energy generation should be used as part of such a station. For example, if there was a sunless season, wind generators or hydroelectric power plants could compensate for this shortage. Rapid adaptability to environmental conditions and consumption volume is one of the main distinguishing features of a virtual power plant relative to conventional power plants.

A large amount of different data and commands is transmitted inside the virtual power plant. For this purpose, a highly secure bidirectional connection is used. Such a connection between each individual asset and the power plant allows for a constant data exchange in real time, which in turn allows for timely monitoring of the free capacity of the assets, and hence the entire virtual power plant. This kind of data also allows you to forecast electricity costs in a timely manner and control pricing in the electricity market [25–27].

Within the framework of Industry 4.0, of which Virtual Power Plants are a part, the digitization of electricity is an irreversible process. In modern realities, electricity production is increasingly moving from large power plants powered by fossil fuels to smaller decentralized power plants using alternative energy sources, which are already combined into a common Virtual power plant.

Like various intermediary platforms, such as hotel booking platforms that do not own a single hotel or various car rental services that do not have their own fleet of vehicles, virtual power plants will be a kind of a management tool for interconnected energy assets.

Such an approach to the distribution of electricity can be much more profitable than the one we are used to, because the number of electricity consumers is increasing every day. The number of electric motors and electric vehicles is growing, the number of network hubs and distributed computing centers is increasing. In order to meet all the growing needs for electricity, the decentralization of energy supply and a hybrid approach to obtaining electricity can become key tools in providing the electricity market with all the necessary assets.

Prepayment system

For full-fledged decentralization and the formation of a full-fledged electricity market, reliable and convenient ways to pay for this energy and some currencies that will embody a certain amount of energy being bought or sold are needed.

If we take a living example from European countries, the UK has taken a big step forward in this matter and introduced prepaid meters.

But in this particular example there are some disadvantages:

1. The operation of their counters is based on smart cards, the balance of which can be replenished and from which funds are debited for a certain amount of energy spent. This approach implies some physical medium, the use of which is not always convenient and cost-effective.

2. Such smart cards are not convenient because in order to replenish them, you need to contact special replenishment points, which, in turn, entails time and sometimes financial costs.

3. One of the main problems is the renewal of meter tariffs. On older samples, this happens manually, which can take quite a long time. This entails situations when the new tariff becomes less profitable, but the consumers lack this information and fail to calculate the costs properly, with inadequate funds debited from the smart cards at the end of the month.

4. There is no bidirectional energy exchange channel in this system. This does not allow end users to act as an energy supplier.

5. Finally, the problem lies in the fact that the tariff payment is monthly. This eliminates the opportunity to save on energy and build a correct plan for its consumption.

Some of these problems can be solved by implementing a token-based prepayment system. For example, we can introduce some equivalent transfer from rubles to a unit of energy exchange and call it Watt (Wt). These will be conditional virtual units of payment for physical energy. For example, you can open a personal account in your name and store a certain amount of Wt on it. Since this currency is not physical, then the costs of its production, maintenance and storage are minimal [28–30].

This approach can be compared to the work of the banking system, in which a separate virtual power plant can act as a bank. The introduction of various mobile applications allowed banks to reduce their financial costs for maintaining the system and at the same time allowed users to manage their financial

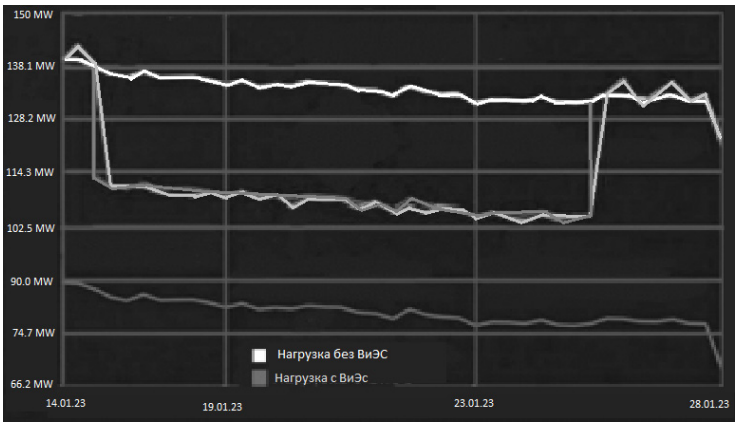

Fig. 4. Modeling of a system with and without VPP

affairs from anywhere in the world, at any time and transparently monitor all transactions with their accounts [31–33].

In the concept of Virtual Power Plants, it is possible to create a system similar to a banking system, where Wt will be the single currency. The storage of this currency on the account allows the consumer to secure the right to receive the appropriate amount of electricity. End users will be able to buy, sell and replenish the amount of Wt that they have on their accounts, and it will also be possible to exchange this virtual currency in a ratio of 1 to 1 for real electricity [34–35]. As an example, the beGateway organization uses this system and provides it to various organizations. In addition, some of the cryptocurrencies (Bitcoin, Ethereum etc.) can also be taken as tokens.

Results

To demonstrate the advantages of the virtual power plant operation, a simulation was carried out based on the indicators of the Dutch power plant with and without the use of virtual power plant technology. The simulation results can be seen on the graph (Fig. 4).

As can be seen from the graph, using the technology of a Virtual Power Plant (VPP), it is possible to obtain the released power within 20 MW. Of course, these indicators may vary depending on the terrain and related technologies. The released capacity can be transferred to other areas where there is a shortage.

For greater convenience and universal use of these systems, convenient mobile applications are being developed. It is necessary that this application is available for any type of installation: both through the APK file and through the built-in applications of Play Market, Apple Store and others. We have developed a blank mobile application that will provide the most understandable user interaction with the virtual power plant service.

Authorization can be done by phone number using the method of double authentication (Fig. 5).

The main page should be as clear as possible for the user and should not overload them with a large amount of information (Fig. 6).

The Kotlin language was used to develop the mobile application. Development was carried out according to the MVP pattern and the CRUD paradigm. Since the application is under development, at the moment its functionality is limited to several functions:

1) User authorization
2) Balance monitoring
3) Linking bank cards to your account
4) Security Settings
5) Display usage statistics

At the moment, there are no applications aimed at solving this problem on the market.

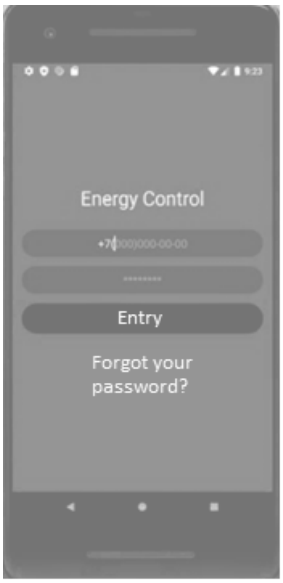

Fig. 5. Authentication screen

Fig. 6. The main application screen

Conclusion

The approach to obtaining and distributing electricity using virtual power plant technology is advanced and promising. It has many advantages:

1. Reduction of electricity tariffs. This solution allows each individual to regulate the required amount of electricity received, which allows optimizing the consumption of excess capacity.

2. Improved forecasting of electricity generation. Thanks to information from users' electronic accounts, it is possible to predict the consumption and the required amount of energy produced.

3. Consumer convenience. Mobile applications and a convenient format of interaction with the system of virtual power plants will allow us to form the most convenient way to exchange the existing data.

REFERENCES

1. **Guan T., Lin H., Sun Q., et al.** Optimal configuration and operation of multi-energy complementary distributed energy systems, Energy Procedia, 2018, Vol. 152. Pp. 77–82. DOI: 10.1016/j.egypro.2018.09.062

2. **Shklyarskiy Y.E., Batueva D.E.** Operation mode selection algorithm development of a wind-diesel power plant supply complex. Journal of Mining Institute, 2022, Vol. 253. DOI: https://doi: 10.31897/PMI.2022.7

3. AutoGrid Virtual Power Plant. Available: https://www.auto-grid.com/products/ virtual-power-plant/ (accessed 16.03.2020).

4. **Safiullin R.N., Afanasyev A.S., Reznichenko V.V.** The Concept of Development of Monitoring Systems and Management of Intelligent Technical Complexes, Journal of Mining Institute, 2019, Vol. 237. DOI: https:// doi: 10.31897/pmi.2019.3.322

5. **Kakran S., Chanana S.** Smart operations of smart grids integrated with distributed generation, A review: Renewable and Sustainable Energy Reviews, 2018, Vol. 81, Part 1. Pp. 524–535. DOI: 10.1016/j.rser.2017.07.045

6. **Yakovleva T.A., Romashev A.O., Mashevsky G.N.** Digital technologies for optimizing the dosing of flotation reagents during flotation of non-ferrous metal ores. Mining Informational and Analytical Bulletin, 2022, Vol. 6 (2). Pp. 175–188. DOI: https://doi:10.25018/0236_1493_2022_62_0_175

7. **Aman M.A., Abbasi M.Z., Ali M., et al.** To Negate the influences of Un-deterministic Dispersed Generation on Interconnection to the Distributed System considering Power Losses of the system, Journal of Mechanics of Continua and Mathematical Sciences, 2018, Vol. 13 (3), Pp. 117–132.

8. **Abramovich B.N., Bogdanov I.A.** Improving the efficiency of autonomous electrical complexes of oil and gas enterprises, Journal of Mining Institute, 2021, Vol. 249. DOI: https:// doi: 10.31897/PMI.2021.3.10

9. **Fishov A., Shiller M., Dekhterev A., et al.** Stability Monitoring and Control of Generation Based on the Synchronized Measurements in Nodes of Its Connection, Journal of Energy and Power Engineering, 2015, Vol. 9. Pp. 59–67. DOI: 10.17265/1934-8975/2015.01.007

10. **Beloglazov I., Krylov K.** An Interval-Simplex Approach to Determine Technological Parameters from Experimental Data. Mathematics, 2022, Vol. 10. DOI: https://doi: 10.3390/math101

11. **Ivanin O.A., Director L.B.** The Use of Artificial Neural Networks for Forecasting the Electric Demand of Stand-Alone Consumers, Thermal Engineering, 2018, Vol. 65, no. 5. Pp. 258–265. DOI: 10.1134/S004060151805004X

12. **Ushakov E., Aleksandrova T., Romashev A.** Neural network modeling methods in the analysis of the processing plant's indicators, 2021. DOI: https://doi:10.1007/978-3-030-57453-6_4

13. **Howell S., Rezgui Y., Hippolyte J.-L.** Towards the next generation of smart grids: Semantic and holonic multi-agent management of distributed energy resources, Renewable and Sustainable Energy Reviews, 2017, Vol. 77. Pp. 193–214. DOI: 10.1016/j.rser.2017.03.107

14. **Sychev Y.A., Zimin R.Y.** Improving the quality of electricity in the power supply systems of the mineral resource complex with hybrid filter-compensating devices. Journal of Mining Institute, 2021, Vol. 247. DOI: https://doi: 10.31897/PMI.2021.1.14

15. **Sha A., Aiello M.** Topological Considerations on Decentralised Energy Exchange in the Smart Grid, Procedia Computer Science, 2018, Vol. 130. Pp. 720–727.

16. **Zakharov L.A., Martyushev D.A., Ponomareva I.N.** Predicting dynamic formation pressure using artificial intelligence methods. Journal of Mining Institute, 2022, Vol. 253, Pp. 23–32. DOI: https://doi.org/10.31897/PMI.2022.11

17. **Marah R., Hibaoui A.E.** Algorithms for Smart Grid management, Sustainable Cities and Society, 2018, Vol. 38. Pp. 627–635. DOI: 10.1016/j.scs.2018.01.041

18. **Yakovleva T.A., Romashev A.O., Mashevsky G.N.** Digital technologies for optimizing the dosing of flotation reagents during flotation of non-ferrous metal ores. Mining Informational and Analytical Bulletin, 2022, Vol. 6 (2), Pp. 175–188. DOI:10.25018/0236_1493_2022_62_0_175

19. **Novykh A.V., Mendez Perez J.A., Gonzalez-Diaz B., Sviridenko I.I., Gogolev G.V., Timofeev V.A.** Increasing the Efficiency of Hybrid Power Plants Using Accumulating Devices. Energeticheskie ustanovki i tekhnologii [Power Plants and Technologies], 2018, Vol. 4, no. 3, Pp. 58–66. (in Russ.)

20. **Nurgalieva K.S., Abdullah K.A., Seyed M.A., Slavko N., John William G.G.** Application of Neural Network and Time-Domain Feature Extraction Techniques for Determining Volumetric Percentages and the Type of Two Phase Flow Regimes Independent of Scale Layer Thickness Applied Sciences, 2022, Vol. 12. Pp. 1–13.

21. **Ushakov E., Aleksandrova T., Romashev A.** Neural network modeling methods in the analysis of the processing plant's indicators, 2021. DOI: 10.1007/978-3-030-57453-6_4

22. **Filippov Ye.V., Zakharov L.A., Martyushev D.A., Ponomareva I.N.** Reproduction of reservoir pressure by machine learning methods and study of its influence on the cracks formation process in hydraulic fracturing. Journal of Mining Institute, 2022, Vol. 258, Pp. 924–932. DOI: https://doi.org/10.31897/PMI.2022.103

23. **Shamil I.R., Grigoriev A., Beloglazov I.I., Savchenkov S.A., Gudmestad O.T.** Research risk factors in monitoring well drilling – A case study using machine learning methods, Symmerty, 2021, Vol. 13, no. 7, Pp. 1–19. DOI: https://www.mdpi.com/2073-8994/13/7/1293

24. **Sultanbekov R.R., Beloglazov I.I., Islamov S.R., Ong M.C.** Exploring of the Incompatibility of Marine Residual Fuel: A Case Study Using Machine Learning Methods, Energies, 2021, Vol. 14, no. 8422, Pp. 1–16.

25. **Brilliant L.S., Zavialov A.S., Danko M.U., Andronov K.A., Shpurov I.V., Bratkova V.G., Davydov A.V.** Integration of machine learning methods and geological and hydrodynamic modeling in field development design.Neftyanoe Khozyaystvo – Oil Industry, 2022, Vol. 3, Pp. 48–53. DOI: 10.24887/0028-2448-2022-3-48-53

26. **Romashev A.O., Nikolaeva N.V., Gatiatullin B.L.** Adaptive approach formation using machine vision technology to determine the parameters of enrichment products deposition. Journal of Mining Institute, 2022, Vol. 256, Pp. 677–685. DOI: https://doi.org/10.31897/PMI.2022.771

27. **Lutonin A., Shklyarskiy J.** Topology and control algorithms for a permanent magnet synchronous motor as a part of a vehicle with in-wheel motors. In P roceedings of the E3S Web of Conferences. EDP Sciences, 2021, Vol. 266, Pp. 04001.

28. **Holkar K., Waghmare L.M.** An overview of model predictive control. International Journal of control and automation, 2010, Vol. 3, Pp. 47–63.

29. **Brigadnov I., Lutonin A., Bogdanova K.** Error State Extended Kalman Filter Localization for Underground Mining Environments.Symmetry, 2023, Vol. 15. DOI: https://doi.org/10.3390/sym15020344

30. **Yu S., Fang F., Liu Y., Liu J.** Uncertainties of virtual power plant: Problems and Countermeasures. Applied Energy, 2019, Vol. 239, Pp. 454–470.

31. **Yavuz Levent, et al.** Transformation of microgrid to the virtual power plant – a comprehensive review. IET generation, transmission & distribution, 2019, Vol. 13, no. 11, Pp. 1994–2005.

32. **Yan Q., Zhang M., Lin H., Li W.** Two-stage adjustable robust optimal dispatching model for multi-energy virtual power plant considering multiple uncertainties and carbon trading. Journal of Cleaner Production, 2022, Vol. 336, Pp. 130400.

33. **Pasetti M., Rinaldi S., Manerba D.** A virtual power plant architecture for the demand-side management of smart prosumers. Applied Sciences, 2018, Vol. 8, No. 3, Pp. 432.

34. **Baringo A., Baringo L.** A stochastic adaptive robust optimization approach for the offering strategy of a virtual power plant. IEEE Transactions on Power Systems, 2016, Vol. 32, no. 5, Pp. 3492–3504.

35. **Kasaei Mohammad Javad, Majid Gandomkar, Javad Nikoukar.** Optimal management of renewable energy sources by the virtual power plant. Renewable Energy, 2017, Vol. 114, Pp. 1180–1188.

INFORMATION ABOUT AUTHORS / СВЕДЕНИЯ ОБ АВТОРАХ

Kozhubaev Yuriy N.
Кожубаев Юрий Нургалиевич
E-mail: y.n.kozhubaev@gmail.com
ORCID: https://orcid.org/0009-0006-1822-7117

Kazanin Dmitriy S.
Казанин Дмитрий Сергеевич
E-mail: um-urii@rambler.ru
ORCID: https://orcid.org/0000-0003-0218-9604

Submitted: 15.06.2023; Approved: 13.12.2023; Accepted: 15.12.2023.
Поступила: 15.06.2023; Одобрена: 13.12.2023; Принята: 15.12.2023.

Computing, Telecommunication and Control, 2023, Vol. 16, No. 4, Pp. 49–59.
Информатика, телекоммуникации и управление. 2023. Том 16, № 4. С. 49–59.

System Analysis and Control
Системный анализ и управление

Research article
DOI: https://doi.org/10.18721/JCSTCS.16405
UDC 681.51

PROJECTION OPERATOR FOR SOLVING GENERALIZED PROBLEMS OF PROGRAM MOTIONS STABILIZATION

A.A. Efremov ✉

Peter the Great St. Petersburg Polytechnic University,
St. Petersburg, Russian Federation

✉ Artem.Efremov@spbstu.ru

Abstract. Generalization and development of the projection operator method for solving problems of stabilization of given program motions seems to be an actual direction of research in the field of synthesis of optimal control systems for nonlinear dynamic stationary objects with limited phase coordinates and controls. In this paper, we formulate generalized stabilization problems for program motions given by a program-stabilizing vector C0 and a vector of admissible program motions C. We show the derivation of a projection operator for solving the specified class of problems. For a nonlinear locally controlled difference operator, admissible controls are synthesized that stabilize program motions under restrictions on phase coordinates and controls. An operator of a dynamical system is obtained for generalized problems of stabilization of program motions with restrictions on the vectors of phase coordinates and controls. Numerical simulation of the stabilization of the given program motions of a dynamic object is carried out. As an example of a dynamic object, a mathematical model of a synchronous generator is chosen, consisting of a system of bilinear differential equations with parameters corresponding to equations in the form of V. A. Venikov. A computational experiment confirmed the theoretical results obtained in the work.

Keywords: projection operators, stabilization of program motions, dynamical systems, optimization, nonlinear difference operator, locally admissible controls, restrictions on phase coordinates and controls

Citation: Efremov A.A. Projection operator for solving generalized problems of program motions stabilization. Computing, Telecommunications and Control, 2023, Vol. 16, No. 4, Pp. 49–59. DOI: 10.18721/JCSTCS.16405

Научная статья
DOI: https://doi.org/10.18721/JCSTCS.16405
УДК 681.51

ПРОЕКЦИОННЫЙ ОПЕРАТОР РЕШЕНИЯ ОБОБЩЕННЫХ ЗАДАЧ СТАБИЛИЗАЦИИ ПРОГРАММНЫХ ДВИЖЕНИЙ

А.А. Ефремов ✉

Санкт-Петербургский политехнический университет Петра Великого,
Санкт-Петербург, Российская Федерация

✉ Artem.Efremov@spbstu.ru

Аннотация. Обобщение и развитие проекционно-операторных методов для решения задач стабилизации заданных программных движений представляется актуальным направлением исследования в области синтеза систем оптимального управления нелинейными динамическими стационарными объектами с ограниченными фазовыми координатами и управлениями. В работе сформулированы обобщенные задачи стабилизации программных движений, заданных программным стабилизирующим вектором C0 и вектор допустимых программных движений C. Показан вывод проекционного оператора решения указанного класса задач. Для нелинейного локально управляемого разностного оператора объекта синтезированы допустимые управления, стабилизирующие программные движения при ограничениях на фазовые координаты и управления. Получен оператор динамической системы для обобщенных задач стабилизации программных движений с ограничениями на векторы фазовых координат и управлений. Проведено численное моделирование стабилизации заданных программных движений динамической объекта. В качестве примера динамического объекта выбрана математическая модель синхронного генератора, состоящая из системы билинейных дифференциальных уравнений с параметрами, соответствующими уравнениям в форме В.А. Веникова. Вычислительный эксперимент подтвердил теоретические результаты, полученные в работе.

Ключевые слова: проекционные операторы, стабилизация программных движений, динамические системы, оптимизация, нелинейный разностный оператор, локально допустимые управления, ограничения на фазовые координаты и управления

Для цитирования: Efremov A.A. Projection operator for solving generalized problems of program motions stabilization // Computing, Telecommunications and Control. 2023. Т. 16, № 4. С. 49–59. DOI: 10.18721/JCSTCS.16405

Introduction

Stabilization of program motions of dynamic objects is an urgent task of modern control theory [1–5]. Methods of inverse dynamics problems [6], Lyapunov barrier functions [7–9], mathematical programming [10, 11], etc. [12–15] are used to solve the problems of stabilization of program motions.

The projection operator method of mathematical programming is used in the paper to solve the specified class of problems [16]. The projection operator method is a universal technique of synthesis of locally admissible and quasi-optimal controlled nonlinear dynamic objects. The generalization and development of the projection operator method for solving tasks of stabilization of given program motions is a relevant research direction in the field of synthesis of optimal control systems for nonlinear dynamic objects with limited phase coordinates and controls.

1. Formulation of generalized problems of stabilization of program motions with inequality constraints on their vector

Generalized problems of stabilization of program motions, specified by the program-stabilizing vector $\mathbf{C}_0$ and the vector of permissible program motions $\mathbf{C}$ have the form: calculate vector

$$\mathbf{x}_* = \arg\min\left\{\varphi(\mathbf{x}) = \left\|\mathbf{x}-\mathbf{C}_0\right\|^2 \middle| \mathbf{A}\mathbf{x}=\mathbf{b},\ \mathbf{A}\in\mathbf{R}^{m\times n},\ \mathbf{C}_0^{\mathrm{T}}\mathbf{C}_0\in\mathbf{D}_x,\right.$$
$$\left.\mathbf{D}_x = \left\{\mathbf{x}\middle|(\mathbf{x}-\mathbf{C})^{\mathrm{T}}(\mathbf{x}-\mathbf{C})\le r^2\right\}\right\}\in\mathbf{R}^n, \tag{1}$$

where $\mathbf{C}_0\in\mathbf{R}^n$ is the stabilizing program vector of state coordinates, $\mathbf{C}\in\mathbf{R}^n$ is the vector of permissible program motions for inequality constraints, $\mathbf{C}_0 < \mathbf{C}$.

Problems (1) generalize the requirements for the problems of stabilization of given program motions [16] by introducing a class of inequality class restrictions $(\mathbf{x}-\mathbf{C})^{\mathrm{T}}(\mathbf{x}-\mathbf{C})\le r^2$, which makes it possible to set more "flexible" requirements for these problems.

2. Synthesis of a projection operator for solving generalized problems of stabilization of program motions

Lemma 1 provides the derivation of the projection operator for solving generalized problems of program motions stabilization (1).

Lemma 1. The projection operator for solving the generalized problem (1) has the form:

$$\mathbf{x} = \mathbf{P}^{+}\mathbf{b} + (1+\lambda)^{-1}\mathbf{P}^0\mathbf{C}_0 + \lambda(1+\lambda)^{-1}\mathbf{P}^0\mathbf{C}, \tag{2}$$

where $\mathbf{P}^0 = \mathbf{E}_n - \mathbf{A}^{\mathrm{T}}\left(\mathbf{A}\mathbf{A}^{\mathrm{T}}\right)^{-1}\mathbf{A}$ is a projector onto a linear manifold $\mathbf{A}\mathbf{x} = \mathbf{b}$, $\mathbf{P}^{+} = \mathbf{A}^{\mathrm{T}}\left(\mathbf{A}\mathbf{A}^{\mathrm{T}}\right)^{-1}$ is a projector onto the orthogonal complement of a linear manifold. The scalar parameter λ is a Lagrange multiplier to restrict the type of inequality in (1).

Proof. The Lagrange function for problem (1) has the form:

$$L = \left\|\mathbf{x}-\mathbf{C}_0\right\|_2^2 + \lambda_0^{\mathrm{T}}(\mathbf{A}\mathbf{x}-\mathbf{b}) + \lambda\left((\mathbf{x}-\mathbf{C})^{\mathrm{T}}(\mathbf{x}-\mathbf{C}) - r^2\right). \tag{3}$$

The necessary conditions for Lagrange optimality are given in the form:

$$L'_x = 2(\mathbf{x}-\mathbf{C}_0) + \mathbf{A}^{\mathrm{T}}\lambda_0 + 2\lambda(\mathbf{x}-\mathbf{C}) = 0_n, \tag{4}$$

$$L'_{\lambda_0} = \mathbf{A}\mathbf{x}-\mathbf{b} = 0_m, \tag{5}$$

$$L'_{\lambda} = (\mathbf{x}-\mathbf{C})^{\mathrm{T}}(\mathbf{x}-\mathbf{C}) - r^2 = 0_1. \tag{6}$$

The necessary optimality condition (4) multiplied by matrix $\mathbf{A}$, considering equality (5) of the form $\mathbf{A}\mathbf{x} = \mathbf{b}$, determines the equation

$$2\mathbf{b} + 2\lambda\mathbf{b} - 2\mathbf{A}\mathbf{C}_0 + \mathbf{A}\mathbf{A}^{T}\lambda_0 - 2\lambda\mathbf{A}\mathbf{C} = 0_n. \tag{7}$$

Then from (7) follows a set of transformations that determines the scalar parameter λ_0, which is the Lagrange multiplier for restricting the type of equality in problem (1).

$$\lambda_0 = 2\lambda\left(\mathbf{A}\mathbf{A}^{T}\right)^{-1}\mathbf{A}\mathbf{C} + 2\left(\mathbf{A}\mathbf{A}^{T}\right)^{-1}\mathbf{A}\mathbf{C}_0 - 2(\lambda+1)\left(\mathbf{A}\mathbf{A}^{T}\right)^{-1}\mathbf{b}. \tag{8}$$

Substituting the Lagrange multiplier λ_0 into (4) and equivalent transformations determine an equation of the form:

$$\mathbf{x} + \lambda\mathbf{x} - \mathbf{C}_0 + \lambda\mathbf{A}^{\mathrm{T}}\left(\mathbf{A}\mathbf{A}^{T}\right)^{-1}\mathbf{A}\mathbf{C} + \mathbf{A}^{\mathrm{T}}\left(\mathbf{A}\mathbf{A}^{T}\right)^{-1}\mathbf{A}\mathbf{C}_0 - (\lambda+1)\mathbf{A}^{\mathrm{T}}\left(\mathbf{A}\mathbf{A}^{T}\right)^{-1}\mathbf{b} - \lambda\mathbf{C} = 0_n.$$

Replacing the projectors $\mathbf{P}^{+}$ and $\mathbf{P}^0$ with subsequent transformations makes it possible to obtain an expression that defines the projection operator for solving problem (1) as a function of the Lagrange multiplier λ for conditions of the type inequality:

$$\mathbf{x} = \mathbf{P}^{+}\mathbf{b} + \left(1+\lambda\right)^{-1}\mathbf{P}^{0}\mathbf{C}_{0} + \lambda\left(1+\lambda\right)^{-1}\mathbf{P}^{0}\mathbf{C}.$$

Lemma is proven.

Next, we consider the solution of generalized problems of stabilization of program motions (1) in the case of equality of the stabilizing program vector of state coordinates and the vector of permissible program motions for inequality constraints $\mathbf{C}_0 = \mathbf{C}$.

Consequence. In the case of equality of the stabilizing program vector of state coordinates and the vector of permissible program motions for inequality constraints $\mathbf{C}_0 = \mathbf{C}$, the solution of generalized problems of program motions stabilization (1) does not depend on the Lagrange multiplier for conditions of the inequality type λ and has the form

$$\mathbf{x} = \mathbf{P}^{+}\mathbf{b} + \mathbf{P}^{0}\mathbf{C}. \tag{9}$$

Proof. Let us repeat the reasoning of Lemma 1 with the condition of equality of the stabilizing program vector of state coordinates and the admissible vector of program coordinates-controls $\mathbf{C}_0 = \mathbf{C}$. Problem (1) will take the form:

$$\begin{gathered}\mathbf{x}_{*} = \arg\min\left\{\varphi(\mathbf{x}) = \left\|\mathbf{x}-\mathbf{C}\right\|^{2} \middle| \mathbf{A}\mathbf{x} = \mathbf{b},\ \mathbf{A}\in\mathbf{R}^{m\times n},\ \mathbf{C}^{\mathrm{T}}\mathbf{C}\in\mathbf{D}_{x},\right. \\ \left.\mathbf{D}_{x} = \left\{\mathbf{x}\middle|\left(\mathbf{x}-\mathbf{C}\right)^{\mathrm{T}}\left(\mathbf{x}-\mathbf{C}\right)\le r^{2}\right\}\right\}\in\mathbf{R}^{n},\end{gathered} \tag{10}$$

Lagrange function for problem (10):

$$L = \left\|\mathbf{x}-\mathbf{C}\right\|_{2}^{2} + \lambda_{0}^{\mathrm{T}}\left(\mathbf{A}\mathbf{x}-\mathbf{b}\right) + \lambda\left(\left(\mathbf{x}-\mathbf{C}\right)^{\mathrm{T}}\left(\mathbf{x}-\mathbf{C}\right) - r^{2}\right). \tag{11}$$

The necessary conditions for function (11) have the form:

$$L_{x}' = 2\left(\mathbf{x}-\mathbf{C}\right) + \mathbf{A}^{\mathrm{T}}\lambda_{0} + 2\lambda\left(\mathbf{x}-\mathbf{C}\right) = 0_{n}, \tag{12}$$

$$L_{\lambda_0}' = \mathbf{A}\mathbf{x}-\mathbf{b} = 0_{m}, \tag{13}$$

$$L_{\lambda}' = \left(\mathbf{x}-\mathbf{C}\right)^{\mathrm{T}}\left(\mathbf{x}-\mathbf{C}\right) - r^{2} = 0_{1}. \tag{14}$$

The first equation (12) multiplied by matrix $\mathbf{A}$, considering equality (13) of the form $\mathbf{A}\mathbf{x} = \mathbf{b}$, determines the equation

$$2\mathbf{b} - 2\mathbf{A}\mathbf{C} + \mathbf{A}\mathbf{A}^{T}\lambda_{0} + 2\lambda\mathbf{b} - 2\lambda\mathbf{A}\mathbf{C} = 0_{n}. \tag{15}$$

Then the scalar parameter is expressed from the resulting equation λ_0,

$$\lambda_{0} = 2\lambda\left(\mathbf{A}\mathbf{A}^{\mathrm{T}}\right)^{-1}\mathbf{A}\mathbf{C} + 2\left(\mathbf{A}\mathbf{A}^{\mathrm{T}}\right)^{-1}\mathbf{A}\mathbf{C} - 2\lambda\left(\mathbf{A}\mathbf{A}^{\mathrm{T}}\right)^{-1}\mathbf{b} - 2\left(\mathbf{A}\mathbf{A}^{\mathrm{T}}\right)^{-1}\mathbf{b}. \tag{17}$$

Substituting λ_0 into (12) followed by opening the parentheses determines the equation:

$$\mathbf{x} + \lambda\mathbf{x} = \mathbf{A}^{\mathrm{T}}\left(\mathbf{A}\mathbf{A}^{T}\right)^{-1}\mathbf{b} + \lambda\mathbf{A}^{T}\left(\mathbf{A}\mathbf{A}^{T}\right)^{-1}\mathbf{b} - \mathbf{A}^{\mathrm{T}}\left(\mathbf{A}\mathbf{A}^{T}\right)^{-1}\mathbf{A}\mathbf{C} - \lambda\mathbf{A}^{T}\left(\mathbf{A}\mathbf{A}^{T}\right)^{-1}\mathbf{A}\mathbf{C} + \lambda\mathbf{C} + \mathbf{C}.$$

Reducing similar ones and substituting the projection operators $\mathbf{P}^{+}$ and $\mathbf{P}^{0}$, allows us to obtain an expression that determines the projection operator for solving problem (10), which does not depend on the Lagrange multiplier λ:

$$\mathbf{x} = \mathbf{P}^{+}\mathbf{b} + \mathbf{P}^{0}\mathbf{C}.$$

Consequence is proven.

3. Synthesis of a dynamic system with restrictions on phase coordinates and controls

This is a method for synthesizing locally admissible controls for the generalized problem of stabilizing a single stationary equilibrium position or program motions specified by the stabilizing program vector $\mathbf{C}_0 = \mathbf{C}_{0k}$ and limited by the vector of admissible program motions $\mathbf{C} = \mathbf{C}_k$, $k \in N$, for an object in the form of a difference operator with restrictions on phase coordinates and controls. In this case, it is assumed that the nonlinear control object is locally controllable according to N.N. Petrov [17–20].

Let a nonlinear locally controlled object be defined by a difference operator:

$$\mathbf{x}_{k+1} = \mathbf{H}\left(\mathbf{x}_k\right) + \mathbf{F}\mathbf{u}_k, \quad \mathbf{y}_k = \mathbf{c}_y\mathbf{x}_k, \quad \mathbf{x}_{k_0} = \mathbf{x}_0 \in \mathbf{D}, \tag{15}$$

where $\mathbf{D} \subset \mathbf{R}^n$ is the neighborhood of attraction as a set of initial states from which the system returns to the equilibrium position. Vectors and matrices of operator (15) have the form $\mathbf{x}_{k+1} \in \mathbf{R}^n$, $\mathbf{x}_k \in \mathbf{D} \subset \mathbf{R}^n$, $\mathbf{y}_k \in \mathbf{R}^l$, $\mathbf{u}_k \in \mathbf{R}^m$, $\mathbf{F} \in \mathbf{R}^{n\times m}$, $\mathbf{c}_y \in \mathbf{R}^{l\times n}$; $\mathbf{H}\left(\mathbf{x}_k\right) \in \mathbf{R}^n$ is the function vector.

Then the linear manifold for the operator optimization problem, considering the difference operator (15), will be written in the form:

$$\mathbf{A}\mathbf{z}_k = \left[\mathbf{E}\middle|-\mathbf{F}\right] \times \begin{bmatrix} \mathbf{x}_{k+1} \\ \mathbf{u}_k \end{bmatrix} = \mathbf{H}\left(\mathbf{x}_k\right) = \mathbf{b}_k, \tag{16}$$

where the object operator, the vector "state-control" and the vector of the right side of the linear manifold have the form:

$$\mathbf{A} = \left[\mathbf{E}\middle|-\mathbf{F}\right] \in \mathbf{R}^{n\times(n+m)}, \ \mathbf{z}_k = \left[\mathbf{x}_{k+1}\middle|\mathbf{u}_k\right]^{\mathrm{T}} \in \mathbf{R}^{(n+m)}, \ \mathbf{b}_k = \mathbf{H}\left(\mathbf{x}_k\right) \in \mathbf{R}^n.$$

Representing the difference operator of an object in the form of a linear manifold (16) allows one to synthesize locally admissible controls by reducing the problem of calculating controls to a countable number of projection operator optimization problems. In this case, the problem of finite-dimensional mathematical programming (1), considering the linear manifold (16), is transformed into a problem of the form: calculate the "generalized" state-control vector (17)

$$\begin{aligned} \mathbf{z}_k^* \triangleq \begin{bmatrix} \mathbf{x}_{k+1}^* \\ \mathbf{u}_k^* \end{bmatrix} = \arg\min \left\{ \varphi\left(\mathbf{z}_k\right) = \left\|\mathbf{z}_k - \mathbf{C}_{0k}\right\|^2 \middle| A\mathbf{z}_k = \left[\mathbf{E}_1\middle|-\mathbf{F}\right] \begin{bmatrix} \mathbf{x}_{k+1} \\ \mathbf{u}_k \end{bmatrix} = \right. \\ \left. = \mathbf{H}\left(\mathbf{x}_k\right) = \mathbf{b}_k, \ \mathbf{C}_{0k} \in \mathbf{D}_z, \ \mathbf{D}_z = \left\{ \mathbf{z}_k \middle| \left(\mathbf{z}_k - \mathbf{C}_k\right)^T \left(\mathbf{z}_k - \mathbf{C}_k\right) \le r^2 \right\}^2 \right\} \in \mathbf{R}^{m+n}, \end{aligned} \tag{17}$$

where $\mathbf{C}_{0k} \in \mathbf{R}^n$ is the stabilizing program vector of state coordinates, $\mathbf{C}_k \in \mathbf{R}^n$ is the vector of permissible program motions for inequality constraints, $\mathbf{C}_k < \mathbf{C}_{0k}$.

The countable set of solutions to mathematical programming problems (17) determines the "state-control" vectors. The structure of the admissible control operator is determined by the generalized projection operator of finite-dimensional optimization (2) and has the form:

$$\mathbf{z}_k^*\left(\varsigma_i, \sigma_i\right) = \mathbf{P}^{+}\mathbf{b}_k + \varsigma_i\mathbf{P}^{0}\mathbf{C}_{0k} + \sigma_i\mathbf{P}^{0}\mathbf{C}_k, \ i = 1, \ 2,$$

where $\varsigma_1 = \left(1+\lambda_1\right)^{-1}$, $\varsigma_2 = \left(1+\lambda_2\right)^{-1}$, $\sigma_1 = \lambda_1\left(1+\lambda_1\right)^{-1}$, $\sigma_2 = \lambda_1\left(1+\lambda_2\right)^{-1}$, λ_1, λ_2 are a pair of Lagrange multipliers for a condition of the inequality type of the problem (1).

The solution vector of the optimization problem under consideration is defined as the image of a convex linear combination of two "boundary generalized operators" $\mathbf{z}_k^*(\varsigma_1, \sigma_1)$ and $\mathbf{z}_k^*(\varsigma_2, \sigma_2)$,

$$\begin{gathered}\hat{\mathbf{z}}_k(\varsigma_1, \varsigma_2, \sigma_1, \sigma_2, \theta) = \theta \mathbf{z}_k^*(\varsigma_1, \sigma_1) + (1-\theta)\mathbf{z}_k^*(\varsigma_2, \sigma_2), \quad \theta \in [0;1], \\ \mathbf{z}_k^*(\varsigma_i, \sigma_i) = \mathbf{P}^+\mathbf{b}_k + \varsigma_i \mathbf{P}^0 \mathbf{C}_{0k} + \sigma_i \mathbf{P}^0 \mathbf{C}_k, \quad i = 1,\ 2.\end{gathered} \tag{18}$$

Vector $\hat{\mathbf{z}}_k(\varsigma_1, \varsigma_2, \sigma_1, \sigma_2, \theta)$ in (18) includes vectors of locally admissible controls $\mathbf{u}_k = \mathbf{T}_u \hat{\mathbf{z}}_k(\varsigma_1, \varsigma_2, \sigma_1, \sigma_2, \theta)$ and vectors of phase coordinate predictions $\mathbf{x}_{k+1} = \mathbf{T}_x \hat{\mathbf{z}}_k(\varsigma_1, \varsigma_2, \sigma_1, \sigma_2, \theta)$ "filtered" using matrices $\mathbf{T}_u = \left[0_{m\times n} \middle| \mathbf{E}_{m\times m}\right]$ and $\mathbf{T}_x = \left[\mathbf{E}_{n\times n} \middle| 0_{n\times m}\right]$ respectively.

As a result, it follows from relations (15)–(18) that the operator of a nonlinear dynamic system with feedback for generalized problems of stabilization of program motions with restrictions on the vectors of phase coordinates and controls specified by the program stabilizing vector $\mathbf{C}_{0k}$ and the vector of permissible program motions $\mathbf{C}_k$ is written as:

$$\begin{gathered}\mathbf{x}_{k+1} = \mathbf{H}(\mathbf{x}_k) + \gamma \mathbf{F} \mathbf{T}_u \hat{\mathbf{z}}_k(\varsigma_1, \varsigma_2, \sigma_1, \sigma_2, \theta), \\ \hat{\mathbf{z}}_k(\varsigma_1, \varsigma_2, \sigma_1, \sigma_2, \theta) = \left[\theta\left(\mathbf{P}^+\mathbf{b}_k + \varsigma_1 \mathbf{P}^0 \mathbf{C}_{0k} + \sigma_1 \mathbf{P}^0 \mathbf{C}_k\right)\right] + (1-\theta)\left(\mathbf{P}^+\mathbf{b}_k + \varsigma_2 \mathbf{P}^0 \mathbf{C}_{0k} + \sigma_2 \mathbf{P}^0 \mathbf{C}_k\right),\end{gathered} \tag{19}$$

where $\varsigma_1 = (1+\lambda_1)^{-1}$, $\varsigma_2 = (1+\lambda_2)^{-1}$, $\sigma_1 = \lambda_1(1+\lambda_1)^{-1}$, $\sigma_2 = \lambda_2(1+\lambda_2)^{-1}$, $\gamma \in R$ – feedback parameter, θ – "acceptability" parameter, $\theta \in [0;1]$.

4. Computational experiment

The section presents the results of a computational experiment of the dynamic system under study with restrictions on phase coordinates and controls (19).

As an example of a dynamic object, we used a vector-matrix bilinear differential model of a synchronous generator [21] with parameters of the Gorev-Park system of equations in the form of V.A. Venikov [22]. To calculate the values of the vector-matrix model, the technical parameters of the TBB-320-2 synchronous turbogenerator were used [23]:

$$\begin{bmatrix} i_d' \\ i_q' \\ i_f' \\ i_{rd}' \\ i_{rq}' \\ \omega' \\ \varphi' \end{bmatrix} = \begin{bmatrix} -3.05 i_d + 9.65 \omega i_q - 0.22 i_f - 2.8 i_{rd} - 5.78 i_{rq} \\ -6.18 \omega i_d - 1.95 i_q + 3.7 \omega i_f + 3.7 \omega i_{rd} - 5.99 i_{rq} \\ -0.98 i_d + 3.1 \omega i_q - 1.92 i_f + 5.32 i_{rd} - 1.85 \omega i_{rq} \\ -3.59 i_d + 11.35 \omega i_q + 1.55 i_f - 10 i_{rd} - 6.79 \omega i_{rq} \\ -8.64 \omega i_d - 2.73 i_q + 5.18 \omega i_f + 5.18 \omega i_{rd} - 10 i_{rq} \\ 67.34 i_q i_d - 67.34 i_d i_q - 40.32 i_q i_f - 40.32 i_q i_{rd} + 40.32 i_d i_{rq} - 4.03 \omega \\ \omega \end{bmatrix} +$$

$$+ \begin{bmatrix} -5.78 & 0 & 0.22 & 0 & 0 & 0 & 0 \\ 0 & -3.7 & 0 & 0 & 0 & 0 & 0 \\ -1.85 & 0 & 1.92 & 0 & 0 & 0 & 0 \\ -6.8 & 0 & -1.55 & 0 & 0 & 0 & 0 \\ 0 & -5.18 & 0 & 0 & 0 & 0 & 0 \\ 0 & 0 & 0 & 0 & 0 & 40.32 & 0 \\ 0 & 0 & 0 & 0 & 0 & 0 & 0 \end{bmatrix} \times \begin{bmatrix} u_d \\ u_q \\ u_f \\ 0 \\ 0 \\ M_{mx} \\ 0 \end{bmatrix}. \tag{20}$$

Discretization of the mathematical model of a synchronous generator (20) is carried out by difference operators of the implicit Euler method [24], implemented in the environment for dynamic modeling of technical systems SimInTech[1].

When conducting a computational experiment, the limitation parameter in the condition of inequality r is taken equal to 1. Feedback parameter $\gamma = -0.001$. The Lagrange multipliers for limiting the type of inequality and the "admissibility" parameter were selected experimentally and are equal to $\lambda_1 = -0.998$, $\lambda_1 = -1.0017$ and $\theta = 0.509$. The generalized vector of stabilization of program motions and controls has the form:

$$\mathbf{C}_{0k} = \left[0 \quad 0 \quad 0 \quad 0 \quad 0 \quad 1 \quad 0 \middle| \quad 0 \quad 0 \quad 0 \quad 0 \quad 0 \quad 0 \quad 0\right]^{\mathrm{T}} \in \mathbf{R}^{14}.$$

Vector $\mathbf{C}_{0k}$ sets the stabilizing value of the synchronous generator frequency ω. The generalized vector of permissible program motions and controls is defined by the equality:

$$\mathbf{C}_{k} = \left[0 \quad 0 \quad 0 \quad 0 \quad 0 \quad 1.001 \quad 0 \middle| \quad 0 \quad 0 \quad 0 \quad 0 \quad 0 \quad 0.03 \quad 0\right]^{\mathrm{T}} \in \mathbf{R}^{14},$$

and in accordance with (20) sets the permissible restrictions on the frequency ω and mechanical torque M_{mx}. To calculate the stresses u_d and u_q, an approximate load model was used [25].

Considering the structure of the linear manifold (16) and the vector-matrix Park–Gorev model for the TBB-320-2 synchronous turbogenerator (20), the calculated projector onto the linear manifold will take the form:

$$\mathbf{P}^0 = \begin{bmatrix}
0.45 & 0 & 0.31 & 0.37 & 0 & 0 & 0 & -0.07 & 0 & 0.09 & 0 & 0 & 0 & 0 \\
0 & 0.33 & 0 & 0 & 0.46 & 0 & 0 & 0 & -0.09 & 0 & 0 & 0 & 0 & 0 \\
0.31 & 0 & 0.66 & -0.18 & 0 & 0 & 0 & -0.04 & 0 & 0.3 & 0 & 0 & 0 & 0 \\
0.37 & 0 & -0.18 & 0.73 & 0 & 0 & 0 & -0.07 & 0 & -0.16 & 0 & 0 & 0 & 0 \\
0 & 0.46 & 0 & 0 & 0.65 & 0 & 0 & 0 & -0.12 & 0 & 0 & 0 & 0 & 0 \\
0 & 0 & 0 & 0 & 0 & 0.99 & 0 & 0 & 0 & 0 & 0 & 0 & 0.02 & 0 \\
0 & 0 & 0 & 0 & 0 & 0 & 0 & 0 & 0 & 0 & 0 & 0 & 0 & 0 \\
-0.07 & 0 & -0.04 & -0.07 & 0 & 0 & 0 & 0.01 & 0 & -0.01 & 0 & 0 & 0 & 0 \\
0 & -0.09 & 0 & 0 & -0.12 & 0 & 0 & 0 & 0.02 & 0 & 0 & 0 & 0 & 0 \\
0.09 & 0 & 0.3 & -0.16 & 0 & 0 & 0 & -0.01 & 0 & 0.15 & 0 & 0 & 0 & 0 \\
0 & 0 & 0 & 0 & 0 & 0 & 0 & 0 & 0 & 0 & 1 & 0 & 0 & 0 \\
0 & 0 & 0 & 0 & 0 & 0 & 0 & 0 & 0 & 0 & 0 & 1 & 0 & 0 \\
0 & 0 & 0 & 0 & 0 & 0.02 & 0 & 0 & 0 & 0 & 0 & 0 & 0.0006 & 0 \\
0 & 0 & 0 & 0 & 0 & 0 & 0 & 0 & 0 & 0 & 0 & 0 & 0 & 1
\end{bmatrix}.$$

The projector onto the orthogonal complement of a linear manifold is defined by the equality:

[1] Dynamic Simulation Environment. Available at: https://simintech.ru

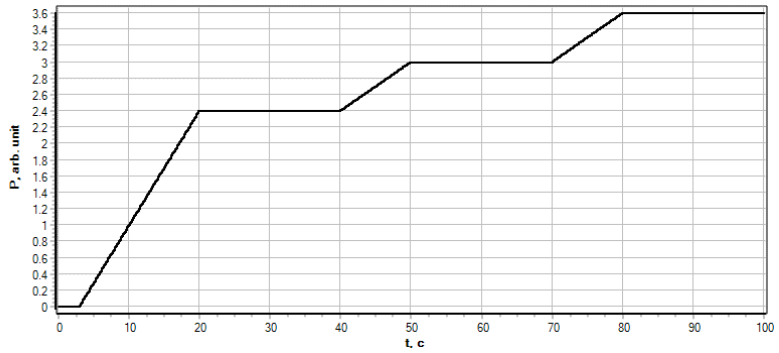

Fig. 1. Power change graph

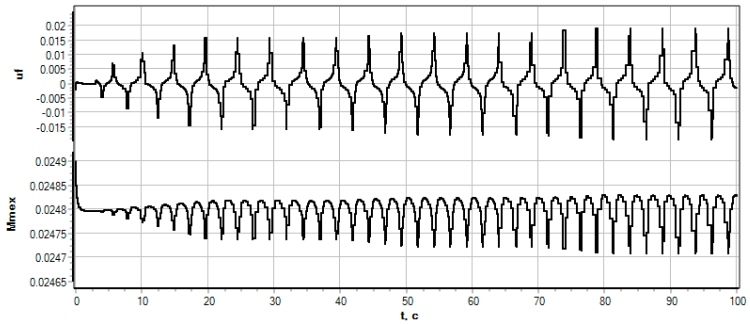

Fig. 2. Synthesized control actions of a synchronous generator
with restrictions specified by the vector of permissible program motions $\mathbf{C}_k$

$$\mathbf{P}^{+} = \begin{bmatrix} 0.55 & 0 & -0.31 & -0.37 & 0 & 0 & 0 \\ 0 & 0.67 & 0 & 0 & -0.46 & 0 & 0 \\ -0.31 & 0 & 0.34 & 0.18 & 0 & 0 & 0 \\ -0.37 & 0 & 0.18 & 0.27 & 0 & 0 & 0 \\ 0 & -0.46 & 0 & 0 & 0.35 & 0 & 0 \\ 0 & 0 & 0 & 0 & 0 & 0.006 & 0 \\ 0 & 0 & 0 & 0 & 0 & 0 & 1 \\ 0.07 & 0 & 0.04 & 0.07 & 0 & 0 & 0 \\ 0 & 0.09 & 0 & 0 & 0.12 & 0 & 0 \\ -0.09 & 0 & -0.3 & 0.16 & 0 & 0 & 0 \\ 0 & 0 & 0 & 0 & 0 & 0 & 0 \\ 0 & 0 & 0 & 0 & 0 & 0 & 0 \\ 0 & 0 & 0 & 0 & 0 & -0.12 & 0 \\ 0 & 0 & 0 & 0 & 0 & 0 & 0 \end{bmatrix}.$$

The graph of changes in the power of a synchronous generator, specified by a piecewise linear function at constant intervals, is shown in Fig. 1.

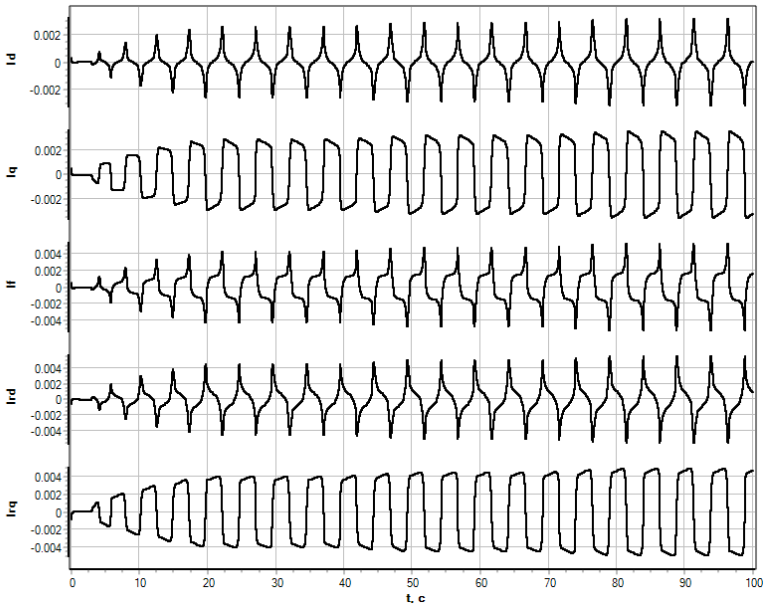

Fig. 3. Dynamics of synchronous generator currents

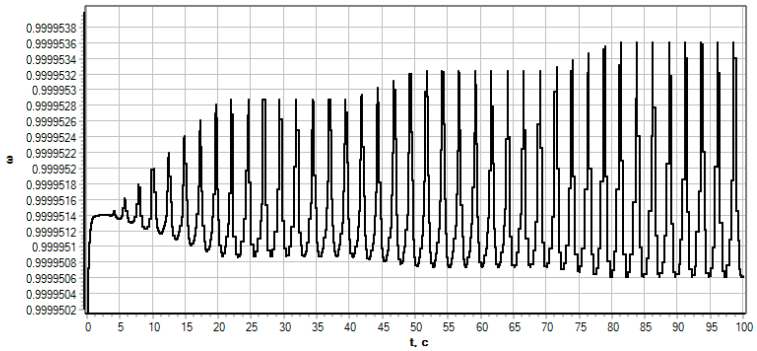

Fig. 4. Dynamics of the permissible change in the "frequency" ω of the synchronous generator, specified by the stabilizing program vector $\mathbf{C}_{k0}$ and the vector of permissible program motions $\mathbf{C}_k$

Limited by the vector of admissible program motions $\mathbf{C}_k$, the locally admissible controls u_f and M_{mx}, defined by operator (19), considering the change in power, have the form shown in Fig. 2.

The dynamics of synchronous generator currents considering the "load graph" (Fig. 1) is shown in Fig. 3.

The dynamics of the permissible change in the "frequency" ω of the synchronous generator, specified by the program stabilizing vector $\mathbf{C}_0$ and limited by the vector of permissible program motions $\mathbf{C}$, considering the "load schedule" (Fig. 1), is shown in Fig. 4.

From Fig. 4 the value of frequency ω, considering the change in power, does not exceed the limitations specified by the vector of permissible program motions $\mathbf{C}_k$.

Conclusions

The paper presents the formulation of generalized problems of stabilization of given program motions and provides the derivation of the projection operator for solving this class of problems.

A dynamic system operator was synthesized for generalized problems of stabilization of program motions with restrictions on the vectors of phase coordinates and controls.

Using the example of a synchronous generator model consisting of a system of bilinear differential equations with parameters corresponding to equations in the form of V.A. Venikov, the use of a synthesized projection operator for calculating controls and stabilizing the phase coordinates of a dynamic system, considering restrictions on coordinates and controls, is demonstrated.

Computational experiments were performed to confirm the correctness of the results obtained.

REFERENCES

1. **Vorob'ev E.I., Mikheev A.V., Morgunenko K.O.** Construction of program motions of relative manipulation mechanisms with three degrees of freedom. Journal of Machinery Manufacture and Reliability, 2019, no. 6, pp. 510–516. DOI: 10.3103/S1052618819060104

2. **Meshchanov A.S., Bikmurzin A.M.** Stabilizatsiya programmnoy posadki letatelnykh apparatov bez shassi na podvizhnuyu platformu v atmosfere pri neopredelennykh vozmeshcheniya. Ch. 1 [Stabilization of program landing of aircraft without landing gear on a moving platform in the atmosphere with uncertain compensation. Part 1.]. Vestnik tekhnologicheskogo universiteta, 2020, vol. 23, № 12, pp. 109–117. (rus)

3. **Alekseev A., Stukonog S.** An algorithm for constructing an optimal ship's path with elements of the ship's program motion systems on the course. Transp. Bus. Russ., 2022, № 2, pp. 217–221. DOI: 10.52375/20728689_2022_2_217/issn2072-8689

4. **Li T., Ren H., Li C.** Intelligent electric vehicle trajectory tracking control algorithm based on weight coefficient adaptive optimal control, Trans. Inst. Meas. Control, 2023, pp. 1–17. DOI: 10.1177/01423312221141591

5. **Yu H., Liang X., H J., F Y.** Adaptive Trajectory Tracking Control for the Quadrotor Aerial Transportation System Landing a Payload Onto the Mobile Platform, IEEE Trans. Ind. Informatics, 2023, pp. 1–12.

6. **Golubev A.Ye.** Stabilizatsiya programmnykh dvizheniy mekhanicheskikh sistem s uchetom ogranicheniy [Stabilization of program motions of mechanical systems considering constraints]. Izvestiya Rossiyskoy akademii nauk. Teoriya i sistemy upravleniya, 2023, № 4, pp. 153–167. (rus) DOI: 10.31857/S0002338823040054

7. **Sachan K., Padhi R.** Lyapunov function based output-constrained control of nonlinear Euler–Lagrange systems. 15th Intern. Conf. on Control, Automation, Robotics and Vision (ICARCV), IEEE, Singapore, November 18–21, 2018, pp. 686–691. DOI: 10.1109/ICARCV.2018.8581068

8. **Wang X., Xu J., Lv M., Zhang L., Zhao Z.** Barrier Lyapunov function-based fixed-time FTC for high-order nonlinear systems with predefined tracking accuracy. Nonlinear Dyn., 2022, vol. 110, no. 1, pp. 381–394. DOI: 10.1007/s11071-022-07627-9/issn0924-090X

9. **Golubev A.Ye.** Postroyeniye programmnykh dvizheniy mekhanicheskikh sistem s uchetom ogranicheniy pri pomoshchi mnogochlenov tretyego poryadka [Construction of program motions of mechanical systems considering restrictions using third-order polynomials]. Izvestiya Rossiyskoy akademii nauk. Teoriya i sistemy upravleniya, 2021, № 2, pp. 126–137. (rus) DOI: 10.31857/S0002338820060049/issn0002-3388

10. **Kozlov V.N., Efremov A.A.** Operators of bounded locally optimal controls for dynamic systems. Lect. Notes Networks Syst. Springer, 2020, vol. 95, pp. 140–145. DOI: 10.1007/978-3-030-34983-7_14

11. **Kozlov V.N., Efremov A.A.** Projection-operator optimization of controls of dynamic objects. J. Phys. Conf., Ser. IOP Publishing Ltd, 2021, vol. 1864, no. 1, pp. 140–145. DOI: 10.1088/1742-6596/1864/1/012076/issn17426596

12. **Kotina Ye.D., Ovsyannikov D.A.** Matematicheskaya model sovmestnoy optimizatsii programmnogo i vozmushchennykh dvizheniy v diskretnykh sistemakh [Mathematical model of joint optimization of program and perturbed motions in discrete systems]. Vestnik Sankt-Peterburgskogo universiteta. Prikladnaya matematika. Informatika. Protsessy upravleniya, 2021, vol. 17, no. 2, pp. 213–224. (rus) DOI: 10.21638/11701/spbu10.2021.210

13. **Andreev A.S., Kolegova L.V.** PID controllers with delay in a problem of stabilization of robotic manipulators' desired motions. Zhurnal Sredn. Mat. Obs., 2022, vol. 34, no. 3, pp. 267–279. DOI: 10.15507/2079-6900.24.202203.267-279/issn20796900

14. **Aleksandrov O.V., Kozik A.A.** Minimaksnaya optimizatsiya parametrov stabilizatsii programmnogo poleta [Minimax optimization of program flight stabilization parameters] // Vestnik Moskovskogo universiteta. Seriya 1. Matematika. Mekhanika, 2019, vol. 3, pp. 45–49. (rus)

15. **Polyanina A.S.** Synthesis of stabilizing control in the generation of multi-body systems program motions, Sovremennyye naukoyemkiye tekhnologii [Modern High Technology], 2020, no. 2, pp. 45–50.

16. **Kozlov V.N.** Proyektsionnyy metod sinteza ogranichennykh optimalnykh upravleniy dinamicheskikh sistem energetiki [Projection method for the synthesis of limited optimal controls of dynamic energy systems]. SPb.: Izd-vo Politekhn. un-ta., 2019. 161 pp. (rus)

17. **Petrov N.N.** Ob upravlyayemosti avtonomnykh sistem [On the controllability of autonomous systems]. Differentsialnyye uravneniya, 1968, vol. 4, no. 4, pp. 606–617. (rus)

18. **Kalman R.E.** Discussion: "On the Existence of Optimal Controls" (Markus, L., and Lee, E.B., 1962, ASME J. Basic Eng., 84, pp. 13–20). J. Fluids Eng., 1962, vol. 84. Available: https://asmedigitalcollection.asme.org/fluidsengineering/article/84/1/21/424598/Discussion-On-the-Existence-of-Optimal-Controls (accessed 30 May 2023).

19. **Avakov Ye.R., Magaril-Ilyayev G.G**. Lokalnaya upravlyayemost i optimalnost [Local controllability and optimality]. Matematicheskiy sbornik, 2021, vol. 212, no. 7, pp. 3–38. (rus) DOI: 0.4213/sm9434

20. **Avakov Ye.R., Magaril-Ilyayev G.G.** Upravlyayemost i neobkhodimyye usloviya optimalnosti vtorogo poryadka [Controllability and necessary conditions for second-order optimality]. Matematicheskiy sbornik, 2019, vol. 210, no. 1, pp. 3–26. (rus) DOI: 10.4213/sm9013

21. **Kozlov V.N., Ryabov G.A., Yefremov A.A., Trosko I.U.** Strukturno-invariantnyye uravneniya energoobyedineniy dlya sinteza sistem ogranicheniya peretokov i regulirovaniya napryazheniya [Structural-invariant equations of power interconnections for the synthesis of flow limitation and voltage regulation systems]. XIX International Scientific and Practical Conference. "System analysis in design and management", St. Petersburg, July 1–3, 2015, pp. 207–217. (rus)

22. **Veretennikov L.P.** Klassifikatsiya uravneniy Goreva–Parka [Classification of Gorev-Park equations]. Elektrichestvo, 1959, no. 11, pp. 13–20. (rus)

23. **Neklepayev B.N.** Elektricheskaya chast elektrostantsiy i podstantsiy. 2-ye izd [Electrical part of power plants and substations. 2nd ed]. M., Energoatomizdat, 1986. (rus)

24. **Skvortsov L.M.** Chislennoye resheniye obyknovennykh differentsialnykh i differentsialno-algebraicheskikh uravneniy [Numerical solution of ordinary differential and differential-algebraic equations]. M.: DMK Press, 2023. (rus)

25. **Leonov G.A., Kuznetsov N.V., Andriyevskiy B.R., Yuldashev M.V., Yuldashev R.V.** Matematicheskoye modelirovaniye perekhodnykh protsessov gidroagregata Sayano-Shushenskoy GES [Mathematical modeling of transient processes of the hydraulic unit of the Sayano-Shushenskaya HPP]. Differentsialnyye uravneniya i protsessy upravleniya, 2018, vol. 4, no. 4. Available: https://diffjournal.spbu.ru/RU/numbers/2018.4/article.1.5.html (accessed: 25.05.2023). (rus)

INFORMATION ABOUT AUTHOR / СВЕДЕНИЯ ОБ АВТОРЕ

Efremov Artem A.
Ефремов Артем Александрович
E-mail: Artem.Efremov@spbstu.ru
ORCID: https://orcid.org/0000-0002-0224-2412

Submitted: 05.09.2023; Approved: 14.11.2023; Accepted: 15.12.2023.
Поступила: 05.09.2023; Одобрена: 14.11.2023; Принята: 15.12.2023.

Computing, Telecommunication and Control, 2023, Vol. 16, No. 4, Pp. 60–69.
Информатика, телекоммуникации и управление. 2023. Том 16, № 4. С. 60–69.

Intellectual Systems and Technologies
Интеллектуальные системы и технологии

Research article
DOI: https://doi.org/10.18721/JCSTCS.16406
UDC 004.932.72

INTEGRATING QUANTITATIVE AND CONVOLUTIONAL FEATURES TO ENHANCE THE EFFICIENCY OF PATHOLOGY CLASSIFICATION IN CT IMAGING

F. Shariaty[1] ✉, *H. Caiqin*[2], *V.A. Pavlov*[1], *L. Duan*[2], *S.V. Zavjalov*[1], *P.T. Pervunina*[3], *W. Ying*[2]

[1] Peter the Great St. Petersburg Polytechnic University, St. Petersburg, Russian Federation;

[2] Jiangsu Normal University, Xuzhou, China;

[3] Almazov National Medical Research Centre, St. Petersburg, Russian Federation

✉ shariaty3@gmail.com

Abstract. The paper proposes an approach that combines radiomic features and deep learning to enhance the accuracy of image classification obtained from lung computed tomography (CT) scans. The deep convolutional neural network ResNet18 was used to extract convolutional features from CT images. Radiomic features describing texture, shape, and intensity were combined with these convolutional features to improve the feature description of the lung CT image dataset. Using Principal Component Analysis (PCA) and feature selection methods, the most informative set of 250 features was obtained. Machine learning models, including Random Forest and Support Vector Machines (SVM), were used for classification. The SVM classifier showed the best results, achieving a classification accuracy of 0.97. The addition of genetic data allowed an improvement in classification accuracy. The study underscores the importance of combining advanced computational methods and data processing methodologies to solve image classification tasks.

Keywords: radiomics; deep learning, machine learning, genetic data, computed tomography scans

Financing: The research was conducted with financial support from the Russian Foundation for Basic Research (RFBR) and the Iran National Science Foundation (INSF) under scientific project number 20-57-56018.

Citation: Shariaty F., Caiqin H., Pavlov V.A. et al. Integrating quantitative and convolutional features to enhance the efficiency of pathology classification in CT imaging. Computing, Telecommunications and Control, 2023, Vol. 16, No. 4, Pp. 60–69. DOI: 10.18721/JCSTCS.16406

Научная статья
DOI: https://doi.org/10.18721/JCSTCS.16406
УДК 004.932.72

ИНТЕГРАЦИЯ КОЛИЧЕСТВЕННЫХ И СВЕРТОЧНЫХ ПРИЗНАКОВ ДЛЯ ПОВЫШЕНИЯ ЭФФЕКТИВНОСТИ КЛАССИФИКАЦИИ ПАТОЛОГИЙ НА ИЗОБРАЖЕНИЯХ КОМПЬЮТЕРНОЙ ТОМОГРАФИИ

Ф. Шариати[1] ✉, *Х. Цайцинь*[2], *В.А. Павлов*[1], *Л. Дуань*[2], *С.В. Завьялов*[1], *Т.М. Первунина*[3], *У. Ин*[2]

[1] Санкт-Петербургский политехнический университет Петра Великого, Санкт-Петербург, Российская Федерация;

[2] Цзянсуский педагогический университет, Сюйчжоу, Цзянсу, КНР;

[3] Национальный медицинский исследовательский центр им. В.А. Алмазова, Санкт-Петербург, Российская Федерация

✉ shariaty3@gmail.com

Аннотация. В работе предложен подход, сочетающий в себе признаки радиомики и глубокого обучения для повышения точности классификации изображений, полученных с помощью компьютерной томографии (КТ) легких. Для извлечения свёрточных признаков из КТ-изображений была использована глубокая свёрточная нейронная сеть ResNet18. Радиомические признаки, описывающие текстуру, форму и интенсивность, были объединены с этими свёрточными признаками для улучшения признакового описания набора данных КТ изображений лёгких. С помощью метода главных компонент (МГК) и методов отбора признаков был получен наиболее информативный набор, состоящий из 250 признаков. Для классификации применялись модели машинного обучения, включая Случайный лес и Метод опорных векторов (МОВ). Классификатор МОВ показал лучшие результаты, достигнув точности классификации 0,97. Добавление генетических данных позволило улучшить точность классификации. Исследование подчёркивает важность объединения передовых вычислительных методик и методологий обработки данных для решения задач классификации изображений.

Ключевые слова: радиомика; глубокое обучение; машинное обучение; генетические данные; компьютерная томография

Финансирование: Исследование проведено при финансовой поддержке Российского фонда фундаментальных исследований (РФФИ) и Национального научного фонда Ирана (INSF) по научному проекту № 20-57-56018.

Для цитирования: Shariaty F., Caiqin H., Pavlov V.A. et al. Integrating quantitative and convolutional features to enhance the efficiency of pathology classification in CT imaging // Computing, Telecommunications and Control. 2023. Т. 16, № 4. С. 60–69. DOI: 10.18721/JCSTCS.16406

Introduction

Algorithms play a central role in many classification tasks, covering a variety of areas. Machine learning methods for non-binary classification are of paramount importance, requiring adaptations to the specific features of each area. In particular, the combination of image processing methods, such as extracting deep convolutional and textural features, allows for analyzing textures in medical images and identifying and classifying pathologies.

Deep convolutional features, formed by convolutional neural networks, are an important component in image processing. Deep learning architectures like ResNet18, ResNet101, and ResNet152 have shown

high performance in feature extraction tasks. These networks are trained to recognize complex image textures, automatically extracting high-level representations, making them invaluable for understanding complex structures in medical images.

Textural features complement deep convolutional features by providing information about variations in pixel intensity and their spatial distribution. These features encompass statistical measures, capturing textural characteristics within images. Methods such as the Gray-Level Co-occurrence Matrix (GLCM), Gabor filters, Local Binary Patterns (LBP), and others study the structure of textures present in images. They enable the identification of areas with significant intensity variations, oriented textures, fine-grained textural differences, and even specific morphological aspects within images.

Existing methods for processing CT images have several notable limitations that require careful consideration [1]. Many modern CT image processing methods primarily rely on image features. These features often lack sufficient depth and informativeness, which can lead to reduced diagnostic accuracy, especially in cases where complex textures in images have diagnostic significance. On the other hand, in some cases, existing methods may not effectively utilize the capabilities of deep learning methods. Deep learning architectures, such as ResNet18, allow for the extraction of convolutional features that can significantly improve diagnostic accuracy [2].

The aim of this work is to combine radiomic and deep convolutional features to develop an algorithm for the detection and classification of cancer in lung CT images [3, 4].

Materials and Methods

Data acquisition

For this study, the NSCLC Radiogenomics dataset was used, which includes CT images of lung patients with various types and stages of lung cancer [6]. This dataset contains medical imaging, genomics, and clinical data. The NSCLC Radiogenomics dataset was prepared with the following objectives:

1. Understanding the genome-image relationships: it serves as a resource for exploring and uncovering the complex relationships between genomic data and characteristics of medical images.

2. Development of prognostic biomarkers: researchers can use this dataset to develop and evaluate prognostic biomarkers of medical images, potentially improving patient stratification and treatment planning. In this study, medical data from 80 patients were used.

In this study, medical data from 80 patients were used.

Feature Extraction

The paper developed a set of features by extracting two types of features: radiomic and convolutional [7]. Let's consider them in detail.

Radiomic features

For the study, 660 radiomic features were extracted for each computed tomography, including first-order features based on shape and texture. Table 1 shows the main texture and shape features extracted from CT images. For further work, 129 different textural features were selected, including Haralick [8], Gray Level Co-occurrence Matrix (GLCM) [9], gradient, Gabor [10], and Local Binary Patterns (LBP).

Haralick Features (based on GLCM): Haralick features were chosen for their ability to detect subtle textural differences in the image. They are particularly useful for identifying fine-grained textural patterns, which may indicate specific pathological features in lung nodules. These features are calculated based on GLCM. For example, one of the Haralick features, contrast, can be calculated as follows:

$$\text{Contrast} = \sum_{i,j} P(i,j) \cdot |i-j|^2,$$

where $P(i,j)$ is the normalized GLCM, i and j are the gray levels in the image.

Other Haralick features have their own equations, but they similarly involve calculations based on the GLCM:

Table 1

Description of the features along with their biological rationale and their association with the morphology of the region of interest (RoI)

Features	Biological rationale and their association with the morphology of the RoI
Gray-Level Co-occurrence Matrix (Texture)	Localizes regions with significant intensity variations within the nodule. It helps identify areas with different textures or patterns inside the RoI
Steerable Gabor (Texture)	Captures oriented textures through changes in direction and scale, which can be useful in describing the microarchitecture or structural patterns within the RoI
Haralick (Texture)	Uses second-order derivatives to capture subtle textural differences in the nodule. It helps in identifying fine-grained textural patterns that may be indicative of certain pathological features
Law (Texture)	Represents spots, ripples, and wave-like appearances in the nodule. These features can be relevant in characterizing specific morphological aspects of the RoI
Fourier (Shape)	This feature involves both low-frequency components, which describe the global shape of the nodule, and high-frequency components, which capture local details or irregularities in the nodule's morphology
Explicit Descriptor (Shape)	This feature includes measures related to contrast, edge sharpness, and the halo effect around the nodule. These aspects can provide insights into the distinctiveness and shape characteristics of the RoI

$$P(i,j)=\frac{N_{ij}}{N_T},$$

where N_{ij} is the number of times a pixel with intensity i is adjacent to a pixel with intensity j in the image, N_T is the total number of pixel pairs in the GLCM, which is equal to the sum of N_{ij} for all possible combinations of i and j.

In other words, $P(i,j)$ quantifies the probability that a pixel with intensity i is adjacent to a pixel with intensity j in the image, considering all possible pixel pairs. This probability is normalized by dividing by the total number of pixel pairs N_T to ensure that $P(i,j)$ represents a probability distribution across all pixel pairs.

2. Gray-Level Co-occurrence Matrix (GLCM) features: GLCM statistics, including Energy, Correlation, and Entropy, are chosen to provide insights into the spatial relationships of pixel intensities within the nodule. These statistics help quantify aspects like uniformity, correlation, and randomness in texture patterns. Common GLCM statistics include:

– Energy:

$$\text{Energy}=\sqrt{\sum_{i,j}P(i,j)^2},$$

– Correlation:

$$\text{Correlation}=\frac{\sum_{i,j}(i-\mu)(j-\mu)P(i,j)}{\sigma_i\sigma_j},$$

– Entropy:

$$\text{Entropy} = -\sum_{i,j} P(i,j) \cdot \log\left(P(i,j)\right),$$

where μ represents the mean or average gray level of the image. It is calculated as follows:

$$\mu = \sum_{i,j} i \cdot P(i,j),$$

3. Gradient: Gradient-based features do not have a single equation but often involve calculating gradients (first-order derivatives) of the image to measure variations in pixel intensities. For example, the magnitude of the gradient can be computed as:

$$\text{Magnitude} = \sqrt{\left(\frac{\partial I}{\partial x}\right)^2 + \left(\frac{\partial I}{\partial y}\right)^2},$$

where (I) is the image, and $\left(\frac{\partial I}{\partial x}\right)$ and $\left(\frac{\partial I}{\partial y}\right)$ are the partial derivatives in the horizontal and vertical directions, respectively.

4. Gabor Features: Gabor filters are defined by a sinusoidal wave modulated by a Gaussian function, and they can be used to extract texture features. The equation for a 2D Gabor filter is:

$$G(x, y; \lambda, \theta, \psi, \sigma, \gamma) = \exp\left(\frac{x'^2 + \gamma^2 y'^2}{2\sigma^2}\right)\cos\left(2\pi\frac{x'}{\lambda} + \psi\right),$$

where (λ) is the wavelength (distance between the peaks of the sinusoidal wave in the Gabor filter), (θ) is the orientation (specifies the orientation angle of the sinusoidal wave in the Gabor filter), (ψ) is the phase offset (introduces a phase shift in the sinusoidal wave), (σ) is the standard deviation of the Gaussian envelope (determines the spread or width of the Gaussian envelope around the sinusoidal wave), (γ) is the aspect ratio (controls the elliptical shape of the filter's Gaussian envelope), and (x') and (y') are rotated coordinates (coordinates represent the spatial location in the image after a rotation by the angle θ). By varying these parameters, Gabor filters can capture different types of texture information.

5. Local Binary Patterns (LBP): LBP is a texture descriptor that encodes the local spatial pattern of pixel intensities. It works by comparing the intensity of a central pixel with its neighbors, classifying each neighbor as either brighter or darker than the central pixel. LBP features can capture patterns such as textures with varying granularity.

Convolutional features

In the study, various deep neural networks were explored for feature extraction from CT images. Specifically, the characteristics of three widely used deep networks, Resnet18 [11], Resnet101 [13], and Resnet152 [14], were compared. The results showed that features extracted from Resnet18 outperformed those from other networks (Resnet101 and Resnet152) in the task of classifying CT images. For this reason, Resnet18 was chosen as the preferred network for feature extraction, which was then combined with radiomic features to create the final feature set. This feature set was used for training machine learning models and assessing their effectiveness in classifying lung CT images for the presence of nodules and their T stage.

Transfer learning was used to fine-tune the pre-trained Resnet18 model on the CT dataset. A 1x512 dimensional vector from the last convolutional layer was extracted as features for each CT image [12].

Feature selection

Statistical analysis and machine learning-based classification were conducted to identify key features with a strong correlation to genetic data. Specifically, a combination of Principal Component Analysis

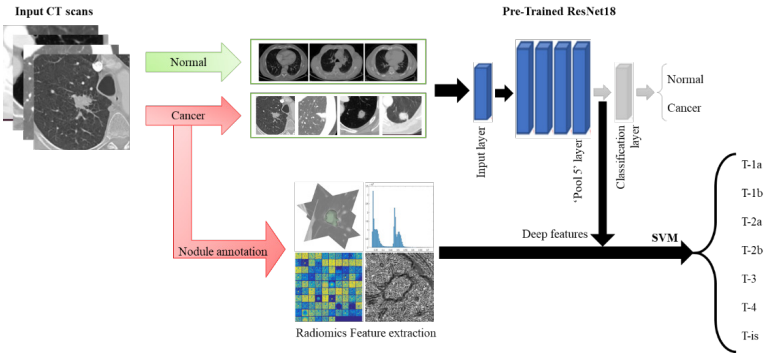

Fig. 1. Flowchart of the proposed method

(PCA) [15] and feature selection methods [16–18] was used to determine the most informative features from the categories of radiomic and convolutional features. Using a combination of PCA and feature selection methods, a set of 250 informative features, including both radiomic and deep features, was determined.

Classification

Subsequently, machine learning models, including Random Forest and Support Vector Machines (SVM) [19–21], were trained to classify lung CT images into seven categories based on the presence of nodules and their T stage. 5-fold cross-validation was used to evaluate the effectiveness of each model. Fig. 1 shows that after obtaining convolutional features, they are combined with radiomic features, which consist of shape, intensity, and texture features. The combined data is then subjected to a classification algorithm to classify them into 7 classes: T-1a, T-1b, T-2a, T-2b, T-3, T-4, T-is.

Experimental Results

The analysis of the lung CT image dataset showed that radiomic and convolutional features are highly informative in predicting the subtype of lung cancer and T stage. Radiomic features are quantitative features reflecting aspects of tumor visualization, including shape, texture, and intensity. On the other hand, convolutional features represent trainable image representations extracted by a pre-trained deep neural network.

The analysis identified a subset of radiomic features, including texture features, which strongly correlate with the genetic heterogeneity of lung cancer. Texture features are sensitive to variations in the spatial distribution of pixel intensities within the tumor and have been shown to be highly informative in predicting tumor heterogeneity and aggressiveness. Using a combination of PCA and feature selection methods, a set of 250 informative features, including both radiomic and deep features, was determined. These features were used to train machine learning models, including Random Forest and SVM classifiers with cubic kernel functions, to classify lung CT scans into seven categories based on the presence of nodules and their T stage.

The combination of convolutional and radiomic features achieved the highest classification accuracy, with an average F1-score of 0.95, Recall of 0.96, and Accuracy of 0.97 across the seven categories. The SVM classifier proved to be the most effective model, achieving an Accuracy of 0.97. These results demonstrate the potential of this approach in improving the accuracy of lung cancer diagnosis and treatment planning. Moreover, the convolutional features extracted using Resnet18 were particularly informative in predicting the presence and T stage of nodules in lung CT scans. This highlights the importance of using deep learning methods in combination with radiomic features for accurate and reliable lung cancer classification.

Overall, the results demonstrate the potential of CT tomography to improve the accuracy of lung cancer classification and provide more precise diagnosis and treatment planning for patients. By identifying

key CT scanning characteristics that have a high correlation, an automatic system was developed for classifying lung CT images into seven categories based on the presence of nodules and their T stage, which can improve patient treatment outcomes and reduce healthcare costs.

Discussion

The results of our study highlight the significant impact of incorporating radiomic features, including texture, shape, and intensity features, in the classification of CT images into seven distinct categories. To understand the relative performance of these features, we compared three different models: Deep Learning (No Radiomics, VGG-16), Deep Learning + Radiomics features, and Deep Learning + Radiomics features + gene data.

When we evaluate the performance of these models, it becomes evident that radiomic features play a vital role in improving the accuracy of CT image classification. The inclusion of radiomic features significantly enhances the F1-Score, Recall, and overall Accuracy of our classification models (Table 2).

Table 2

Comparative Performance of Classification Models

Model	F1-Score	Recall	Accuracy
S.K. Lakshmanaprabu et al. [21]	–	–	0.94
Deep Learning (No Radiomics)	0.75	0.68	0.78
Deep Learning + Radiomics features	0.91	0.88	0.93
Deep Learning + Radiomics features + gene data	0.95	0.96	0.97

Table 2 highlights a significant performance gap between using only deep learning and integrating radiomic features. Notably, the inclusion of genetic data further enhances performance, demonstrating the potential of multidimensional data integration. The invaluable role of radiomic features in improving diagnostic accuracy must be acknowledged. The limitations of the deep learning model without radiomic features can be attributed to its inherent constraints in capturing complex patterns in CT images. Radiomic features, in contrast, provide quantitative insights into tumor characteristics, making them sensitive to variations in pixel intensity and spatial distribution, crucial for predicting tumor heterogeneity and aggressiveness.

In our study, Principal Component Analysis (PCA) and feature selection methods allowed the extraction of a set of 250 informative features, including both radiomic and deep features. These features were essential for training machine learning models, including Random Forest and Support Vector Machines (SVM) with cubic kernel functions, for classifying lung CT scans. The SVM classifier, in particular, emerged as the most effective model, achieving an Accuracy of 0.97. The combination of convolutional and radiomic features achieved the highest classification accuracy, with an F1-score of 0.95, Recall of 0.96, and Accuracy of 0.97 across the seven categories.

Table 2 also shows another study that attempted to classify lung CT images. This approach employed an Optimal Deep Neural Network (ODNN) and Linear Discriminant Analysis (LDA) to analyze lung CT images. Deep features were extracted from these images and LDA was used for dimensionality reduction to classify lung nodules as either malignant or benign. The ODNN was then optimized using a Modified Gravitational Search Algorithm (MGSA) for lung cancer classification. This alternative approach reported an impressive sensitivity of 96.2%, specificity of 94.2%, and accuracy of 94.56%. Compared to this alternative study, our approach, enriched with radiomic features and genetic data, achieves an accuracy of 97%, representing a substantial 3% increase compared to models based on deep learning without radiomics. The addition of radiomic features significantly improved diagnostic accuracy, emphasizing the promise

of combining multi-modal data sources for redefining cancer classification and personalized treatment planning.

Furthermore, the comparison of different deep networks for feature extraction showed that Resnet18 outperforms other architectures, emphasizing its potential as the preferred choice for feature extraction in radiomic studies. Although our study focused on lung cancer classification, the developed approach can be applied to other types of cancer, demonstrating the potential of using multiple data sources, including genetic data and visualization data, to enhance the accuracy of cancer diagnosis and treatment planning. A limitation of our study is the relatively small sample size and manual segmentation. Future research using larger datasets and automated segmentation methods can provide further insights into the potential of our approach for lung cancer classification and personalized treatment planning.

Conclusions

The study aimed to explore the relationship between features based on computed tomography and genetic heterogeneity in lung cancer patients with the goal of improving the accuracy of cancer classification. It was shown that the integration of radiomics and deep learning methods can significantly improve the accuracy of lung cancer diagnosis and treatment planning, while the use of genetic data in combination with visualization data can help identify key features associated with lung cancer.

Adding radiomic features to deep features increased the classification accuracy by 13%, from 78% to 91%. Furthermore, the inclusion of genetic data further improved accuracy by 4%, reaching an impressive 95%. This demonstrates the substantial impact of multidimensional data integration on the performance of our classification models.

Our approach showed high accuracy in predicting the presence and T stage of nodules in lung CT scans, as well as the ability to differentiate between malignant and benign nodules. It was also found that convolutional features extracted using Resnet18 were particularly informative in predicting the presence and T stage of nodules, highlighting the potential of deep learning methods for feature extraction in radiomic studies.

The ability to accurately predict the presence and T stage of nodules in lung CT scans can have significant implications for individualized treatment planning and identifying patients at high risk of developing lung cancer. The study indicates the potential of using multiple data sources to develop automated cancer classification systems and personalized treatment planning to improve patient outcomes and reduce the burden of lung cancer. The obtained results underscore the importance of continuing to develop and refine innovative approaches to cancer diagnosis and treatment planning, with the ultimate goal of improving patient outcomes and reducing the impact of lung cancer on individuals and society.

REFERENCES

1. **Sannasi Chakravarthy S.R., Rajaguru H.** Deep-features with Bayesian optimized classifiers for the breast cancer diagnosis. International Journal of Imaging Systems and Technology, 31 (4) (2021) 1861–1881.

2. **Li W., et al.** Prognosis of male lung cancer patients with urinary cancer: a study from a national population-based analysis. Scientific Reports, 13 (1) (2023) 283.

3. **Baranov M., Velichko E., Shariaty F.** Determination of geometrical parameters in blood serum films using an image segmentation algorithm. Optical Memory and Neural Networks, 29 (2020) 330–335.

4. **Xia T., et al.** Fused feature signatures to probe tumour radiogenomics relationships. Scientific Reports, 12 (1) (2022) 2173.

5. **Bianconi F., et al.** Texture analysis on [18 F] FDG PET/CT in non-small-cell lung cancer: correlations between PET features, CT features, and histological types. Molecular imaging and biology, 21 (2019) 1200–1209.

6. **Bakr S., et al.** A radiogenomic dataset of non-small cell lung cancer. Scientific data, 5 (1) (2018) 1–9.

7. **Shen W., et al.** Learning from experts: developing transferable deep features for patient-level lung cancer prediction. in Medical Image Computing and Computer-Assisted Intervention–MICCAI 2016: 19th International Conference, Athens, Greece, October 17–21, 2016, Proceedings, Part II 19. 2016. Springer.

8. **Haralick R.M., Shanmugam K., Dinstein I.H.** Textural features for image classification. IEEE Transactions on systems, man, and cybernetics, 6 (1973) 610–621.

9. **Nissar A., Mir A.H.** Texture based steganalysis of grayscale images using neural network. Signal processing research, 2 (1) (2013) 17–24.

10. **Grigorescu S.E., Petkov N., Kruizinga P.** Comparison of texture features based on Gabor filters. IEEE Transactions on Image processing, 11 (10) (2002) 1160–1167.

11. **He D.C., Wang L.** Texture features based on texture spectrum. Pattern recognition, 24 (5) (1991) 391–399.

12. **Pavlov V.A., et al.** Application of deep learning techniques for detection of COVID-19 using lung CT scans: model development and validation. in International Youth Conference on Electronics, Telecommunications and Information Technologies: Proceedings of the YETI 2021, St. Petersburg, Russia. 2022. Springer.

13. **Shandilya S., Nayak S.R.** Analysis of lung cancer by using deep neural network. in Innovation in Electrical Power Engineering, Communication, and Computing Technology: Proceedings of Second IEPCCT 2021. 2022. Springer.

14. **Yang J.W., et al.** Classification of subtypes including LCNEC in lung cancer biopsy slides using convolutional neural network from scratch. Scientific Reports, 12 (1) (2022) 1830.

15. **Naseriparsa M., Kashani M.M.R.** Combination of PCA with SMOTE resampling to boost the prediction rate in lung cancer dataset. arXiv preprint arXiv:1403.1949, 2014.

16. **Ge G., Zhang J.** Feature selection methods and predictive models in CT lung cancer radiomics. Journal of Applied Clinical Medical Physics, 24 (1) (2023) e13869.

17. **Skalunova M., Shariaty F., Rozov S., Radmard A.R.** "Personalized Chemotherapy Selection for Lung Cancer Patients Using Machine Learning and Computed Tomography", 2023 International Conference on Electrical Engineering and Photonics (EExPolytech), ST PETERSBURG, Russian Federation, 2023, pp. 128–131, DOI: 10.1109/EExPolytech58658.2023.10318700

18. **Shariaty F., et al.** Texture appearance model, a new model-based segmentation paradigm, application on the segmentation of lung nodule in the CT scan of the chest. Computers in biology and medicine, 140 (2022) 105086.

19. **Shariaty F., Zavjalov S.V., Pavlov V.A., Pervunina T.M., Orooji M.** Inf-Seg: Automatic segmentation and quantification method for CT-based COVID-19 diagnosis. Computing, Telecommuni-cations and Control, 15 (3) (2022) 7–21. DOI: 10.18721/JCSTCS.15301

20. **Shariaty F., et al.** Application of a texture appearance model for segmentation of lung nodules on computed tomography of the chest. Journal of the Russian Universities, 25 (3) (1998) 97.

21. **Lakshmanaprabu S.K., Mohanty S.N., Shankar K., Arunkumar N., Ramirez G.** Optimal deep learning model for classification of lung cancer on CT images. Future Generation Computer Systems, 92 (2019) 374–382.

INFORMATION ABOUT AUTHORS / СВЕДЕНИЯ ОБ АВТОРАХ

Shariaty Faridoddin
Шариати Фаридоддин
E-mail: shariaty3@gmail.com
ORCID: https://orcid.org/0000-0002-7060-8826

Caiqin Han
Цайцинь Хань
E-mail: hancq@jsnu.edu.cn

Pavlov Vitalii A.
Павлов Виталий Александрович
E-mail: pavlov_va@spbstu.ru
ORCID: https://orcid.org/0000-0003-0726-6613

Duan Lingfeng
Дуань Линфэн
E-mail: duan.l0014@gmail.com

Zavjalov Sergey V.
Завьялов Сергей Викторович
E-mail: zavyalov_sv@spbstu.ru
ORCID: https://orcid.org/0000-0003-3398-3616

Pervunina Tatiana M.
Первунина Татьяна Михайловна
E-mail: ptm.pervunina@yandex.ru
ORCID: https://orcid.org/0000-0001-9948-7303

Ying Wu
Ин У
E-mail: wuying@jsnu.edu.cn

Submitted: 12.09.2023; Approved: 14.11.2023; Accepted: 15.12.2023.
Поступила: 12.09.2023; Одобрена: 14.11.2023; Принята: 15.12.2023.